Article

Wide-Area Near-Real-Time Monitoring of Tropical Forest Degradation and Deforestation Using Sentinel-1

Dirk Hoekman [1],*, Boris Kooij [2], Marcela Quiñones [2], Sam Vellekoop [2], Ita Carolita [3], Syarif Budhiman [3], Rahmat Arief [4] and Orbita Roswintiarti [3,4]

[1] Water Systems and Global Change Group, Wageningen University, Droevendaalsesteeg 3, 6708 PB Wageningen, The Netherlands

[2] SarVision, Agro Business Park 10, 6708 PW Wageningen, The Netherlands; kooij@sarvision.nl (B.K.); quinones@sarvision.nl (M.Q.); vellekoop@sarvision.nl (S.V.)

[3] Remote Sensing Applications Center, Jalan Kalisari No.8, Pekayon, Jakarta 13710, Indonesia; ita.carolita@lapan.go.id (I.C.); syarif.budhiman@lapan.go.id (S.B.); orbita@lapan.go.id (O.R.)

[4] Remote Sensing Technology and Data Center, Jalan Lapan No.70, Pekayon, Jakarta 13710, Indonesia; rahmat.arief@lapan.go.id

*   Correspondence: dirk.hoekman@wur.nl; Tel.: +31-317482894; Fax: +31-317419000

check for updates

Abstract: The use of Sentinel-1 (S1) radar for wide-area, near-real-time (NRT) tropical-forest-change monitoring is discussed, with particular attention to forest degradation and deforestation. Since forest change can relate to processes ranging from high-impact, large-scale conversion to low-impact, selective logging, and can occur in sites having variable topographic and environmental properties such as mountain slopes and wetlands, a single approach is insufficient. The system introduced here combines time-series analysis of small objects identified in S1 data, i.e., segments containing linear features and apparent small-scale disturbances. A physical model is introduced for quantifying the size of small (upper-) canopy gaps. Deforestation detection was evaluated for several forest landscapes in the Amazon and Borneo. Using the default system settings, the false alarm rate (FAR) is very low (less than 1%), and the missed detection rate (MDR) varies between 1.9% ± 1.1% and 18.6% ± 1.0% (90% confidence level). For peatland landscapes, short radar detection delays up to several weeks due to high levels of soil moisture may occur, while, in comparison, for optical systems, detection delays up to 10 months were found due to cloud cover. In peat swamp forests, narrow linear canopy gaps (road and canal systems) could be detected with an overall accuracy of 85.5%, including many gaps barely visible on hi-res SPOT-6/7 images, which were used for validation. Compared to optical data, subtle degradation signals are easier to detect and are not quickly lost over time due to fast re-vegetation. Although it is possible to estimate an effective forest-cover loss, for example, due to selective logging, and results are spatiotemporally consistent with Sentinel-2 and TerraSAR-X reference data, quantitative validation without extensive field data and/or large hi-res radar datasets, such as TerraSAR-X, remains a challenge.

Keywords: Sentinel-1; NRT monitoring; deforestation; degradation; tropical forest; tropical peat

1. Introduction

Worldwide, forests disappear at alarming rates. In the last decade, the average annual net forest/non-forest conversion loss was estimated at 4.74 million ha [1]. Degradation of remaining natural forests is another major concern. A recent study of the Amazon region showed that losses in carbon were almost evenly split between cases attributable to forest conversion (e.g., biomass removals

associated with commodity-driven deforestation) and cases due to forest degradation and disturbance (e.g., biomass reductions attributable to selective logging, drought, wildfire, etc.) [2]. Less well-known, but of equal concern, are losses of peat underneath tropical peat swamp forests. The largest tropical peat deposits are found in Indonesia, the Peruvian Amazon, and the Congo Basin, accounting for a total of approximately100 gigatons carbon (GtC), equal to 25% of the carbon stock stored globally in biomass [3–5]. For example, in degraded peat swamp forests in Indonesia, on average, approximately 0.4 GtC is lost annually because of oxidization and fires [6]. Forest loss, forest degradation, and peat degradation are important components of carbon accounting. The Intergovernmental Panel on Climate Change (IPCC) recently released the 2019 Refinement to the 2006 IPCC Guidelines for National Greenhouse Gas Inventories, where the use of Earth observation data plays a prominent role [7]. In addition to its role in carbon accounting, timely information on forest change is needed in support of other applications, such as forest management and peatland restoration. Optical satellite data have been used for decades for forest-change monitoring. Cloud cover, which can be very persistent in tropical rainforests, may pose problems when continuous timelines and timeliness of information is important. Radar data, such as Sentinel-1 data, offers an alternative. Radar's independence of cloud cover is a clear advantage. However, this may not be the only advantage, as is explored later in this paper.

Deforestation is commonly defined as land-use change from forest land to any other non-forest land-use category and forest degradation as long-term loss of forest carbon stocks, as well as forest values without land-use, change [8–11]. However, quantitative criteria to describe forest degradation are still under discussion. Specification of thresholds for carbon stock loss and minimum area and time affected are not given, but are mandatory to apply such a definition [9–11]. Deforestation detection (with optical data) is based on the easy differentiation between forest and non-forest classes, such as open areas, bare soil, agriculture, and settlements. Commonly used methods are based on sub-pixel approaches like spectral mixture analysis, which are also used to assess proxies of forest degradation [12–15]. The abovementioned recent study of the Amazon was based on MODIS data at ~500 m resolution [2]. It states that applying higher-resolution satellite data (e.g., 30 m Landsat imagery) would reduce uncertainty in carbon loss estimates, in particular, from degradation and disturbance. Another study, based on Landsat, mentions that subtle degradation signals are not easy to detect and are quickly lost over time due to fast re-vegetation [16]. This would mean that significant loss of carbon could remain undetected. Obviously, higher spatial resolution provides more detail; however, regrowth or remaining understory can limit disturbance detection. Radar imaging is fundamentally different in several ways and can also be used to detect subtle patterns of forest disturbance, such as patterns caused by selective logging. Good results have been obtained with airborne radar [17], and high-resolution satellite radar data, such as COSMO-SkyMed spotlight data [18] and TerraSAR-X 3 m stripmap data [19,20]. However, such data types are not practical for wide-area monitoring applications. Coarser resolution radar data, such as the Sentinel-1 IW data, may offer a good alternative.

Forest disturbance, either through forest loss or drainage, can result in tropical peat disturbance. Peat swamp forests are among the world's most threatened and least known ecosystems. In Southeast Asia, large areas of peat swamp forest have been drained, deforested (for timber), converted for agricultural projects (even though the soil is too acid), or are converted into plantations (such as oil palm, acacia, and Borneo rubber), even though peat systems are fragile and sensitive to hydrological disturbance (e.g., see Reference [21]). Drainage through canalization has frequently and severely disrupted groundwater-level dynamics. Besides resulting in CO_2 emissions due to oxidization [22,23], this process makes them particularly vulnerable to fire, especially during 'El Niño' years [24]. Emissions from the fires in Indonesia during 1997–1998, for example, have been estimated to be 0.8–2.5 GtC [25,26]. Water management is essential in addressing these disturbances. Indonesia currently makes efforts to restore degraded peatlands by "re-wetting", blocking canals and promoting paludiculture. For these vast areas, near-real-time (NRT) information is needed on the construction of new drainage canals in the forest, which are often illegal and a precursor to further

forest and peat disturbance. This is currently achieved by using SPOT-6/7 and Pleiades data, even though costs and cloud cover pose severe limitations.

Wide-area and spatially detailed NRT data are needed not only for tropical peatland management and restoration. Other sectors needing such data include law enforcement, national forest monitoring systems, and indigenous communities; MRV systems, carbon accounting, and REDD+ projects; sustainable development of timber trade, forest plantations, and other commodities; protection of conservation areas, biodiversity, and ecological corridors; and early warning and disaster management [1,10,27–30].

Several wide-area NRT systems already exist. Since 2004, near-real-time deforestation monitoring over the Brazilian Amazon has been carried out by INPE based on the Real Time Deforestation Detection System (DETER) program. The system currently uses the optical AWiFS data with 56 m spatial resolution and five-day temporal resolution [31]. Because cloud cover poses a problem, the JJ-FAST system is considered as an additional NRT data source [32]. The JJ-FAST system is based on ALOS PALSAR-2 ScanSAR data and is the first SAR-based global early warning system for tropical forests (covering 77 countries) [33,34]. It currently offers deforestation data every 1.5 months, at a minimum mapping unit (MMU) of 2 ha. Validation based on Landsat data provided by the GLAD system [15] shows an overall user accuracy of 66.7% [35]. The ALOS PALSAR observation strategy was designed to provide consistent wall-to-wall observations, at fine resolution, of almost all land areas on Earth, on a repetitive basis [36]. In addition to providing the data for the JJ-FAST system, it is used to make annual global forest/non-forest maps [37] and provide insight in the spatiotemporal radar backscatter variation of tropical forests [38]. The L-band variability is relatively low for (dryland) tropical rainforest, higher for tropical moist deciduous forest and highest for tropical dry forest (for HH-polarization up to 3.5 dB standard deviation). The variability is also high for wetlands, such as peat swamp and floodplain forests [38]. Moreover, for C-band data, spatiotemporal backscatter variation of tropical rainforest is low [39] and can be substantial for tropical dry forest [40].

Though L-band radar, in general, provides better contrast between forest and non-forest classes [41–45]; C-band radar also seems well suitable for forest-change monitoring. From an operational point-of-view, this is particularly true for the Sentinel-1 radar, which reliably provides free medium-resolution data with a global coverage at a 6- or 12-day repeat cycle. From a technical point-of-view, there are a few challenges. (1) The first is the contrast between forest and non-forest, which, compared to L-band, is often low and of short duration (because of regrowth). (2) The spatiotemporal variability of forest can be substantial, notably for wetland forests; however, it seems lower than for L-band. (3) Spatial co-registration, with optical data and other radar, is difficult because of forest height, and limitations of available DEMs and radar parallaxes. This is especially true for the finer details, such as forest edges and disturbances. (4) Radar imaging is fundamentally different from optical imaging. Together with the previous issue, this complicates validation based on other satellite data. (5) Moreover, as stated in Reference [32], "radar image analysis must be conducted carefully because there is no single pattern of deforestation in the Brazilian Amazon". This is also the case for other tropical rainforest areas. Results depend on forest and terrain type and other environmental conditions, as discussed in this paper.

Several recent studies discuss the appropriateness of Sentinel-1 for forest/non-forest discrimination and deforestation detection. For a dryland forest site in the Peruvian Amazon, deforestation could be detected successfully (detection rate 95%) based on time-series analysis of radar shadows and the combined use of ascending and descending observations [43]. In Reference [44], several methods for forest/non-forest classification for a wide range of forest types are discussed. Classification accuracies for the tropical rainforest sites in this study are up to 81.6% (Sumatra) and up to 88.6% (Colombia). In Reference [45] the potential of time-series and recurrence metrics for deforestation mapping at test sites in Mexico is discussed. In Reference [46], for a site in the Amazon, it is shown that (time-series of) interferometric coherence has potential for deforestation detection.

The objective of this paper is to discuss the suitability of Sentinel-1 radar for wide-area, NRT monitoring of tropical forest change in terms of deforestation and degradation, for a variety of landscapes in Indonesia and the Amazon, including tropical peat swamp forest landscapes. This requires clear definitions of forest, deforestation, degradation, and disturbance. However, users in different countries and disciplines use different definitions. It is therefore practical to have a flexible system that can be adapted to the needs of the user. It is also necessary to indicate the limitations of such a system. In this paper, certain default settings and definitions are used. The forest class includes undisturbed and disturbed natural forest and excludes forest plantations, such as acacia, rubber, and eucalypt. Deforestation is defined as clear-cut areas exceeding a certain size. The default threshold is arbitrarily set at 1.0 ha, except for peat swamp forest, where 0.3 ha is used. Any detected forest loss smaller than the default size is labelled as degradation. Degradation in degraded forests is mapped as the additional degradation since the start of the monitoring. The defaults values for the change detection algorithms used in this study were established during earlier work in Malaysia and Sumatra and seem generally applicable in all areas studied so far, including the Guianas, Gabon, and the areas validated in this paper. Special characteristics of tropical peat swamp forests, viz, the flat terrain and occurrence of long and narrow straight gaps caused by drainage canal construction, form ideal conditions for theoretical studies relevant for development of models to quantify degradation. Section 2.1 introduces the study sites and supporting data. Sections 2.2–2.4 describe physical background, system design considerations, and types of errors and summarize system components. Section 2.5 provides a theoretical background for the radar imaging of linear canopy gaps (roads and canals) and small canopy gaps (tree logging gap disturbances) and introduces a physical model for radar imaging at high-resolution. Section 3 provides results for NRT canal gap detection, NRT deforestation monitoring, and NRT degradation monitoring. It also reflects on validation challenges. Sections 4 and 5 provide a synthesis and the main conclusions. The system is tested for a range of tropical forest landscapes and seems to function well, even in challenging environments, such as mountain slopes and wetlands. In this paper, the term "landscape" is used in the context of an ecosystem approach and stands for a vast area with a mosaic of forest types.

2. Materials and Methods

2.1. Study Sites and Supporting Data

The system was tested in several tropical forest areas, comprising wall-to-wall coverage of the island Borneo, Suriname, Guyana, and selected sites in Brazil, Colombia, Gabon, and the island Sumatra, for the entire period of Sentinel-1 observation, since launch (see Tables 6 and 7). System validation mainly focused on the Indonesian Province Central Kalimantan (154,000 km^2) on Borneo and the municipality Almeirim (73,000 km^2) in the State of Pará, Brazil (see Figure 1). These two validation areas have a wide range of forest types, as well as a wide range of deforestation and degradation characteristics. Central Kalimantan was almost entirely covered by tropical evergreen forest until the 1980s. Intensive logging of predominant commercial Dipterocarp species and conversion to cropland, oil palm, and timber plantations has reduced forest cover significantly. Other major natural vegetation types include peat swamp forests, which are found in the coastal and sub-coastal lowlands, freshwater swamps along rivers inland, and mangrove forests in the coastal plains. Large fractions of the peat swamp forests are drained, causing frequent forest fires, notably in El Niño periods. Almeirim, located between the Amazon River and Suriname, has moist evergreen forest, varied topography, and blackwater nutrient-poor rivers. Selective logging and conversion to pasture, agriculture and plantations occur in this area, however, the rates of deforestation and degradation are still relatively low.

Monitoring forest change requires knowledge on the location and characteristics of forest at the start of the monitoring period. A simple approach would be to use the globally available forest/non-forest maps derived from PALSAR-2 [37]. For this study, accurate regional baseline maps with more detailed thematic information were made based on the first available Sentinel-1 images,

and concurrent PALSAR-2, Landsat-8, and, when available, Sentinel-2 images [47–49], using the systematics of the FAO Land Cover Classification System (LCCS) [50]. The combination of these three sensors allows accurate distinction of the different forest classes, such as peat forest, heath forest, high dipterocarp forest, mangrove forest, riparian forest, and forest plantations. The LCCS classification system describes vegetation in terms of vegetation structure and soil wetness conditions, such as flooding under the canopy. L-band radar is able to observe wetness under the canopy and is uniquely suitable to distinguish dryland and wetland forest classes. The baseline typically comprises 30 classes, depending on the eco-region. For Borneo, using 9000 reference areas, an accuracy of 85% was achieved [51]. In combination with additional historical data (mainly PALSAR), additional information on degradation, regrowth, and flood frequency (also under the canopy) is obtained.

(**a**)   (**b**)
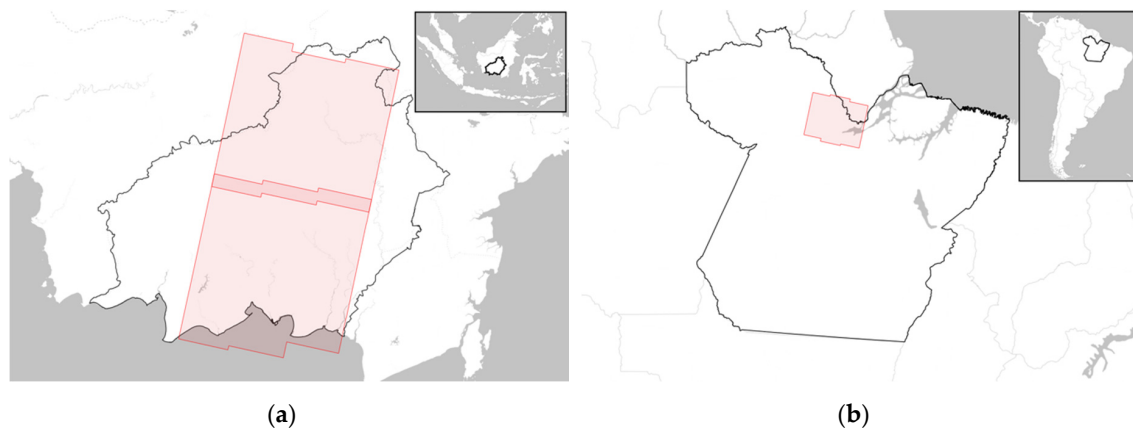
Figure 1. Overview test site locations. Two Sentinel-1 footprints in the Indonesian Province Central Kalimantan (**a**). One Sentinel-1 footprint in Brazilian State of Pará (**b**).

Sentinel-2, SPOT-6/7, Google Earth, and TerraSAR-X single polarization 3 m resolution stripmap data were used to validate the detected forest changes (see Tables 6 and 7). For Sentinel-1 data simulation use was made of field and LiDAR data collected in earlier experiments (see Section 2.5).

2.2. Physical Background of Methodology

In general, undisturbed forests have a relatively high and stable backscatter level; therefore, a significant decrease in backscatter level would indicate deforestation. Though true in general, this assumption, for several reasons, is too simple to allow for accurate change detection, notably for small-scale disturbances and wetland forests. Three reasons are discussed next.

(1) In the first place, good knowledge on the natural temporal backscatter variation of undisturbed forest is required. For tropical rainforests, the causes of natural variation include seasonality, foliage wetness, soil wetness, and flooding. The strengths and spatial scales of these phenomena also depend on the forest type, notably, because of flooding, on the distinction between dryland and wetland forest types. Moreover, rain affects backscatter level, though this strongly depends on rain intensity and radar wavelength. For the C-band of Sentinel-1, for example, heavy rain can result in a slight decrease in backscatter over large areas, while excessive rain can result in backscatter decrease exceeding 3 dB over smaller areas. A typical example is given in Figure 2. Approaches to address temporal backscatter variation are discussed later.

(2) The opposite can also be true. Radar images may not show any clearly perceivable change even though strong forest disturbance has taken place (such as in Figure 20). This phenomenon is partly explained in Figure 3. Logging a single large tree causes a small depression in the upper canopy. A small area of backscatter decrease (caused by radar shadow) and a small adjacent area of backscatter increase (caused by radar overlay) results, even when the lower canopy still covers the soil completely (Figure 3B). The mean backscatter is hardly affected, while the patterns which constitute the texture

change significantly. When the lower canopy is also removed, the radar textural change signal is somewhat stronger (Figure 3C). Optical systems, in the latter case, may detect spectral change because of a bare soil contribution. However, there are two other important differences between radar and optical imaging to consider. The first difference is the duration of change. Since it usually takes years for the canopy gap depression to fill up again, while it only takes a few weeks or months for the bare soil to be covered with regrowth again, radar change is well observable for a long period, while, for optical systems, this is only a short time and only in the absence of cloud cover. The second difference is the incidence angle. Theoretical models (to be discussed in Section 2.5) show that Sentinel-1 incidence angle has little effect, while, for optical systems, this may not be true. Since canopy gaps can be small and deep, incidence angles for optical systems may be too large to observe the soil surface in high forest. For Sentinel-2, the local incidence angle can be as large as 23.86° [52], while, for SPOT-6/7, using the oblique viewing capability, as is often done for areas with persistent cloud cover, this can be as large as 45°. Though the Sentinel-1 signal of a new small gap is stable for a long period, it is also weak. It relates to a few pixels only and the backscatter decrease and increase is roughly at the same level as the standard deviation of the radar speckle. Approaches to estimate this weak signal in the presence of speckle are discussed later.

(3) The backscatter level of clear-cut areas, in both polarizations, is usually significantly lower (>2.0 dB) than the original forest cover. Under certain circumstances, however, factors such as remaining debris and undergrowth, terrain slopes [53], soil roughness, and soil moisture can cause much smaller decreases. This loss of contrast can be temporarily or persistent. It is evident that good knowledge is needed on the causes, levels, and probabilities of contrast loss, for the landscapes to be monitored.

The monitoring system is designed to be capable of accommodating all the above mentioned issues as good as possible; however, at a certain point, compromises have to be made. These compromises are discussed in Section 2.4, after the introduction of the system components in Section 2.3.

(**a**)   (**b**)
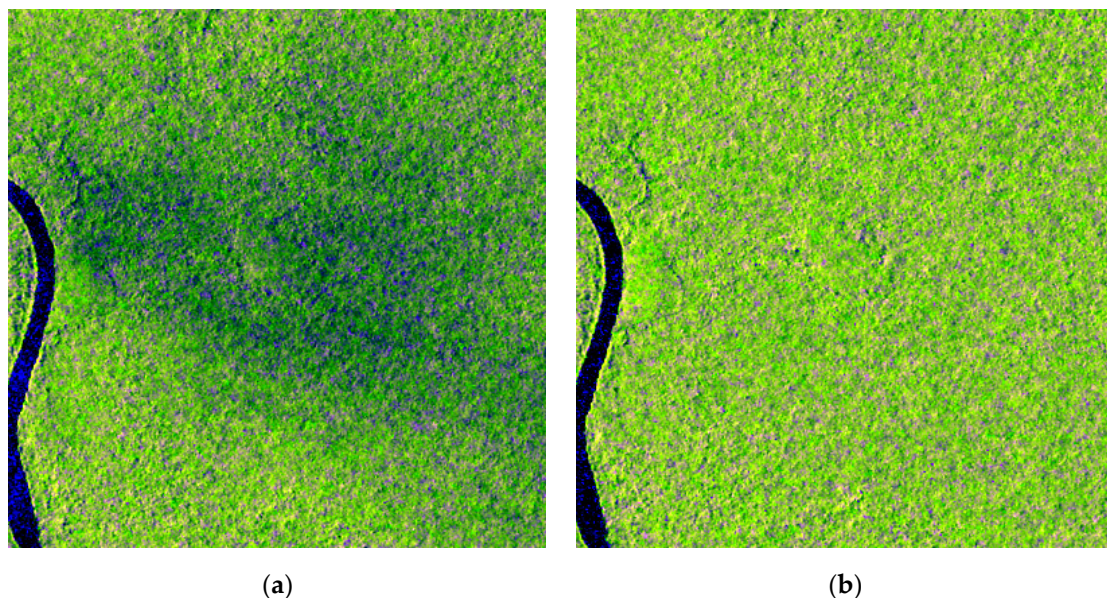
Figure 2. Sentinel-1 radar image of 20161229 (**a**) and next observation at 20170122 (**b**). Excessive rain at the first date reduces backscatter in VV- and VH-polarization with more than 3 dB. Location: Sebangau, Central Kalimantan. Size: 6 km × 6 km. Standard color scale: (red) VV with range −15.0 to −6.0 dB; (green) VH with range −24.0 to −13.0 dB; (blue) VV–VH with range 4.0 to 12.0 dB.
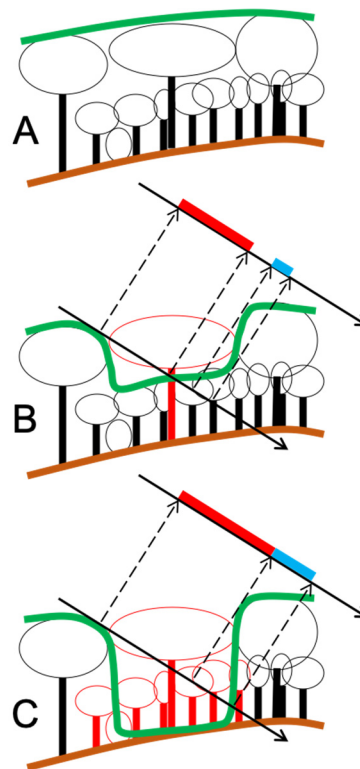
Figure 3. Radar response to forest degradation. Pre-disturbance situation (case **A**). Small gaps create small areas of (dark) "radar shadow" and (bright) "radar overlay", shown in red and cyan, respectively. Therefore, extraction of large canopy trees can be detected, even when the soil is still covered with lower vegetation (case **B**). When a soil fraction is visible (case **C**), both radar and optical detect extraction. The radar signal persists over long periods when canopy gaps are steep and deep.

2.3. System Description

End-to-end system: As soon as a new Sentinel-1 radar image is available [54], the system automatically downloads this image, updates time-series analyses, and produces new maps, including a deforestation map, a forest access-road map, and a forest-degradation map. Since the baseline reference is in the past, and updates have to be made chronologically, the system initially produces a series of historical maps, before commencing near-real-time map production. In this paper, these historical sequences are studied and validated. The end-to-end system consists of many steps. It is out of scope to discuss all of these technical steps in detail. Therefore, only a high-level description and some relevant details are presented next.

Preprocessing: Interferometric preprocessing is performed for radiometric calibration, geometric correction, and precise co-registration. This is done over tiles, each containing 30–50 bursts, covering the landscape (Figure 4). Preprocessing includes slope correction [53] and slant-range multi-temporal speckle reduction. The speckle reduction step combines a number of approaches [55–57] in order to preserve edges and texture well. This is relevant, in particular, for the quality of the access road and forest degradation assessment. Speckle filtering increases the equivalent number of looks (ENL) from 4 to 19 and reduces speckle in homogeneous regions from 2.3 to 1.0 dB. The result is an (updated) time-series of dual-polarization (VV- and VH-) intensity images at a 15 m pixel size and interferometric coherence data. It is noted that, throughout this paper, backscatter intensity is expressed by the backscattering coefficient γ^0 ($\gamma^0 = \sigma^0 / \cos(\theta_{inc})$, where σ^0 is the normalized radar cross-section).
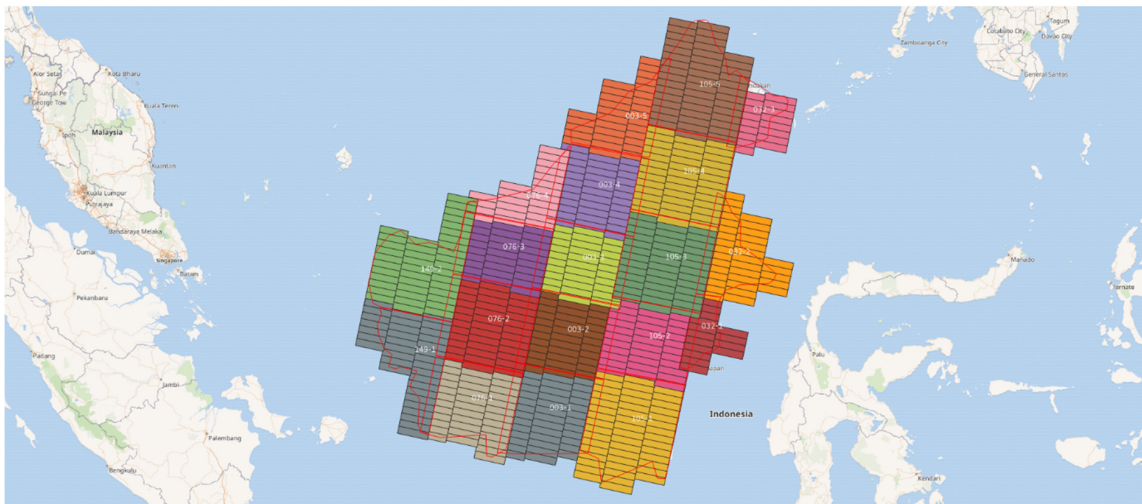
Figure 4. Area division is done in tiles typically comprising 30–50 Sentinel-1 bursts. Borneo Island.

There are two important reasons for using the Single Look Complex (SLC) products instead of the more generally used Ground Range Detected (GRD) products as input data. SLC data are in the original radar geometry and can be converted by multi-looking and orthorectification in the required ground range geometry. However, SLC data also contain phase information which allows for a very precise co-registration (typically 6 mm accuracy) of multi-looked data in the slant range. Another advantage is that all slant-range multi-look pixels have the same ENL, which allows for superior multi-temporal speckle reduction. Co-registration of GRD data is far less precise and typically has an accuracy of several meters in flat areas but can exceed the pixel dimension in mountainous areas. The increased sharpness and spatial co-registration as a result of interferometric preprocessing (i.e., using phase information) is essential to allow the applications as discussed in this paper, in particular, the quantification of degradation and the detection of subtle linear features.

Baselines: The baseline consists of a land-cover baseline map (described in Section 2.1) and a Sentinel-1 reference image from the same date. The land-cover map is used to stratify the landscape, allowing forest-type-dependent algorithm settings for change detection, as well as forest-type-dependent assessment of spatiotemporal backscatter variation in undisturbed forest. The latter assessment is done at a much coarser scales; however, it still captures changes caused by flooding of wetland forest. The backscatter decrease in cells of extreme rainfall cannot be corrected well and has to be dealt with in the thematic mapping steps.

Change detection: When the natural temporal backscatter variation is taken into account, change follows by detecting a substantial backscatter increase or decrease in one or both of the polarizations. Such a change can be flagged (i.e., provisionally detected) by using relatively simple time-series analysis techniques, such as Bayesian techniques [58]. A similar technique is adopted here; however, several important interconnected modifications have been made. (1) Segmentation allows time-series analysis at segment level, not only pixel level. (2) The threshold for change detection is not fixed. It not only depends on forest class and terrain slope angles but can also change in time and in relation to the position in the segment. For example, the threshold can be lowered after a confirmed change detection or for pixels at the edge of a segment. (3) To avoid error propagation and to allow a high sensitivity (i.e., low threshold values), the results of the pixel-based change detection are used in a feedback loop, to regulate the segment-based results. (4) The change is not a scalar value but is defined as the combined vectorial change of the two polarizations. (5) Several minimum mapping unit (MMU) sizes are used, depending on forest type and product type. For example, for deforestation in high dryland dipterocarp forest, the MMU is 1.0 ha, and for peat swamp forest, the MMU is 0.3 ha. Intermediate products with still lower MMUs are made to guide the production of forest-degradation

maps. The latter information can be added to the deforestation maps as a qualitative indication where degradation is ongoing.

Products: The NRT system currently produces, next to the deforestation and degradation maps, two other types of thematic maps. Quantitative forest-degradation maps are based on a theoretical model for radar imaging of canopy gaps. This is discussed in Section 2.5. The third map type is based on change of linear features. It is used to update access road maps and canals, such as in peat swamp forest, and also gives qualitative indications of degradation. This is also discussed in Section 2.5. Consequently, three fundamentally different types of forest-change maps are generated, each focused on different aspects of forest change. A flowchart is shown in Figure 5.
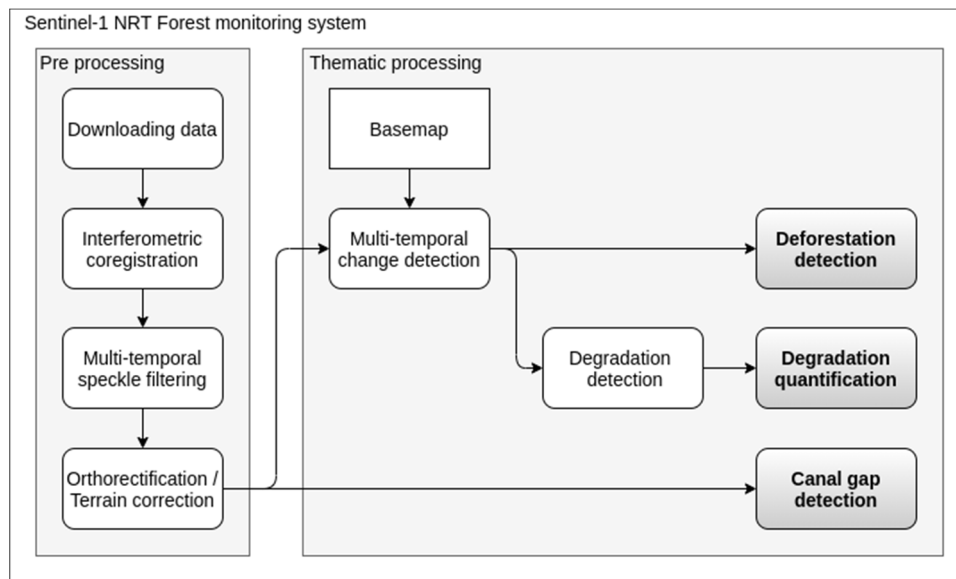
Figure 5. Flowchart: preprocessing and thematic processing steps of the Sentinel-1 near-real-time (NRT) forest-monitoring system.

2.4. Types of Errors and Compromises

For a near-real-time monitoring system, two types of compromises exist. To discuss these, the error types should be introduced first. Suppose Sentinel-1 NRT deforestation maps are validated using available Sentinel-2 images. Two factors would complicate this validation exercise. The first is the asynchrony of the radar and optical time-series and the second is cloud cover. These complications are addressed by defining six rule-based classes as shown in Table 1. Missing pixels in the optical reference dataset, because of clouds and cloud shadows, are classified as forest when the pixel has the forest class in future images and are classified as non-forest when the pixel has the non-forest class in a previous image. The remaining missing pixels are classified as unknown. Only pixels labelled in the baseline as one of the forest classes are evaluated.

Table 1. Quality control classes and color coding used for validation of deforestation.

	CD1	Correct deforestation detection
	CD2	Correct deforestation detection, prior to next optical reference date
	MD	Missed non-forest detection
	UN	Unknown
	CF	Correct forest classification
	FA	False alarm

A pixel or segment is labelled as correct deforestation (CD1) when an optical image of the same or earlier date is deforested. It is also labelled as correct deforestation (CD2) in case the previous

optical image shows the forest class and the next optical image the non-forest class. The label "missed non-forest detection" (MD) is assigned when the pixel is classified as forest in the radar map and non-forest in a previous optical image. The label false alarm (FA) is assigned when the pixel is classified as non-forest in the radar map and as forest in the previous optical image. The label correct forest classification (CF) is assigned when the pixel is classified as forest in the radar map and the previous optical image. Using these rules, not all the radar map pixels can be labelled with one of these five classes because of the presence of unknowns in the optical reference maps. In these cases, the label unknown (UN) is assigned. The false alarm rate (FAR) and missed detection rate (MDR) are calculated by using the following equations:

$$FAR = FA/(FA + CF) \tag{1}$$

$$MDR = MD/(MD + CD1 + CD2) \tag{2}$$

The performance of the system can be tuned to specific needs of the user. Basically, the user has to make two important compromises. The first relates to the interchangeability of the two types of detection error, i.e., the false alarm (FA) rate and the missed detection (MD) rate, also known as false positive and false negative. When algorithm settings are selected to decrease the FA rate, then the MD rate increases, and vice versa. Of course, multiple maps using different settings can be made. The second compromise relates to the interchangeability of overall accuracy and timeliness. The timeliness of NRT maps is defined on the basis of the dates of the available radar image time-series. When the first radar image has the time stamp t_0 (t zero), the second t_1, etc., and the last t_p (t present), then the second to last image has time stamp t_{p-1}. An NRT map can be based on a t_p radar image, a t_{p-1} radar image or, in general, a t_{p-n} radar image. Larger values for *n* cause larger delays in map availability; however, in general, they result in larger overall accuracy. Of course, multiple maps using different values of *n* can be made simultaneously and can be combined. To make a distinction between different types of NRT maps, these are denoted as NRT(N = 0), NRT(N = 1), etc. Within an NRT(N = 1) system the most recent radar image is only used as confirmation, which, for example, can be used to avoid false alarms caused by heavy rain cells. The default NRT system studied in this paper is an NRT(N = 1) system with a low FA rate. Nevertheless, evaluation of the performance of this relatively simple system can yield important insights. These insights, to be presented in this paper, support the design of more accurate and complicated systems which combine multiple maps made with different settings, tuned for the landscapes of interest.

2.5. Theoretical Background of Canal-Gap Mapping and Forest-Degradation Quantification

Models of the physical interaction, the forest structure, and the canal gap geometry can be used to simulate radar imaging of canal gaps. The canal gap geometry was derived from SPOT-6/7 data and is expressed as canal width and orientation. The description of forest structure is based on field observations from previous studies [17,19,59,60]. Relevant parameters include forest height and canopy roughness. The physical interaction is modelled at high resolution, accounting for the three-dimensional structure of canopy roughness and incidence angle, as described in Reference [61] and canal gap geometry.

Radar profiles of canal gaps were extracted from the radar images in the east–west direction by re-sampling and averaging over straight canal sections of approximately 45 radar image rows, which strongly reduces the variation caused by speckle. Figure 6 shows a comparison between an observed profile and a simulated profile. The observation differs from the simulation because of remaining speckle and texture effects. However, across the canal profile, the fit is very good, with a standard error of estimate of only 0.5 dB. Results over several canal sections are summarized in Table 2 and Figure 7. Since realistic simulations can be made, the radar backscatter model can be used as a theoretical tool to support further quantitative analysis. In Section 3.1, this is done to study limiting factors related to canal gap detection and in Section 3.3 to study possibilities to quantify small forest-gap dimensions in relation to forest degradation.
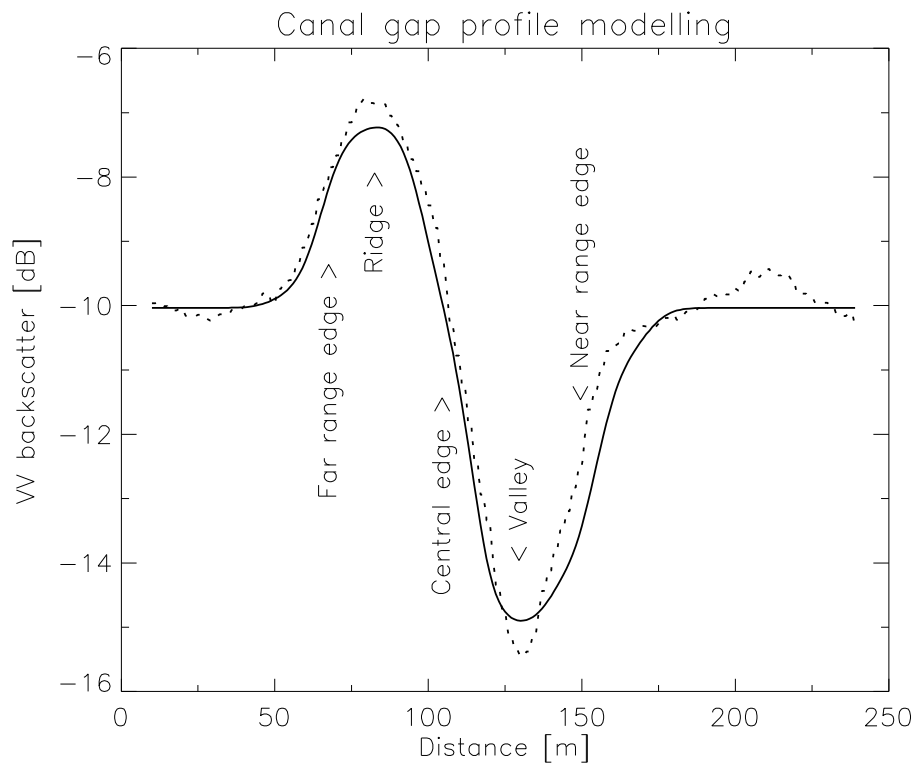
Figure 6. Comparison between simulated radar backscatter profile across a canal gap (solid curve) and an observed profile (dotted curve). The positions of the ridge, valley, and edges are indicated.
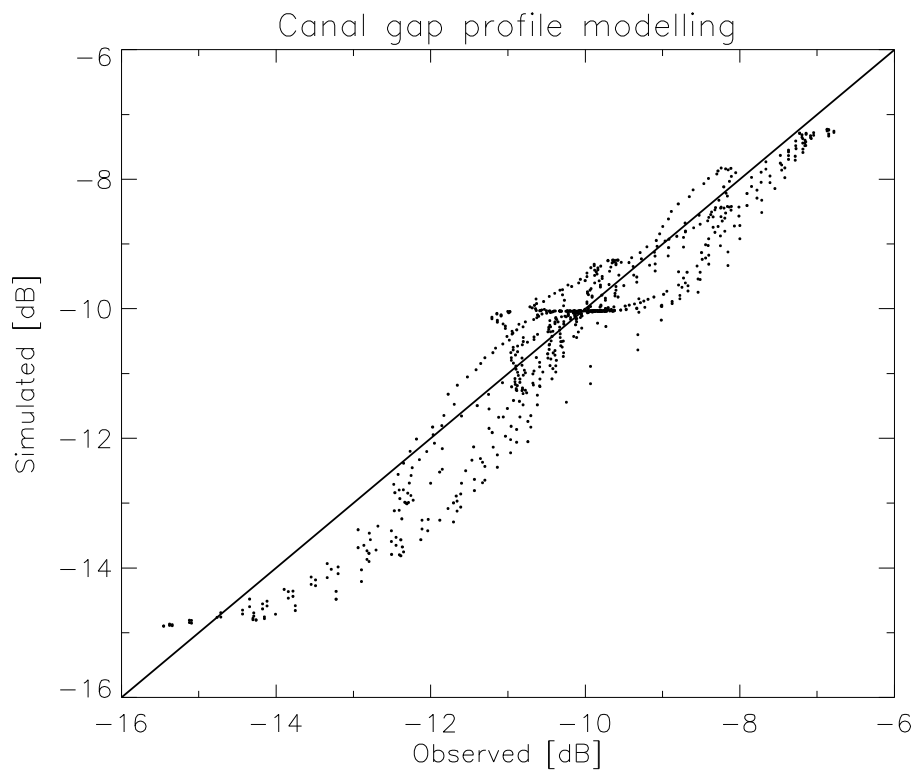
Figure 7. Comparison of observed and predicted VV-backscatter across five canal gaps.

Table 2. Canal gap simulation results. Width of gap (m), orientation with respect to radar azimuth direction (degrees), RMSE (dB), and Pearson correlation between observed and predicted values. Note that the RMSE for canal B is relatively large. This is caused by its large width, which causes visibility of the gap floor, and strong regrowth on the gap floor, which causes an increase in backscatter.

Canal	Width	Orientation	RMSE	r^2
A	56.2	32.6	0.501	0.987
B	50.0	32.6	0.813	0.959
C	32.8	32.4	0.556	0.964
D	25.0	31.3	0.386	0.954
E	18.7	63.4	0.285	0.870
Average			0.539	0.959

Since the radar data are acquired near the equator in descending orbit, the azimuth direction is $-168.0°$ with respect to north and the radar look direction, which is towards the right, is $-78.0°$, i.e., almost west. For descending data, as shown in Figure 6, the radar profile of the canal gap, shows a ridge positioned left of a valley. The valley results from radar shadowing and the ridge from radar overlay. The widths and heights of the ridges and valleys vary as function of canal gap width and orientation. The characteristic shape of the radar gap profile suggests several alternative approaches for linear feature detection. For descending data in the direction from east to west (or right to left) the profile shows a negative edge (or sharp decrease) followed by a valley, a sharp increase, a ridge and a second negative edge. It suggests that several classes of operators are suitable to detect the canal gaps, such as edge detectors, ridge-valley (or line) detectors [62,63], and matching filters (for the characteristic valley-ridge pattern in descending data). The application of these operators is the first step in the process of generating canal-gap maps. Subsequent steps include thresholding of the detections, applying spatial shifts (because the operators act on different parts of the canals gaps), linking small segments into larger segments (by evaluating canal gap directions), and time-series analysis (to reduce false alarms). The operators used for detection are briefly described first.

The Sobel operator was used for edge detection. It uses two 3×3 kernels which are convolved with the original image to calculate approximate edge gradients in the horizontal and vertical direction. In subsequent steps, for computational efficiency, the edge gradients in only eight discrete directions (at 45-degree intervals) are used. Therefore, in the initial step, eight 3×3 kernels are applied as shown in Figure 8 (top). The same approach was used for the ridge and valley detection (see Figure 8, middle) and the matched filter detection (Figure 8, bottom). Therefore, in this approach, in total, 24 types of detection per pixel can be made. Since these detections are not independent, a selection of a subset of these detections would be sufficient. A careful evaluation showed that 10 types suffice without decreasing performance and that the main value of the matched filter is the improvement of the detection of small canals. The latter also explains the shape of the matched filter, which works well on narrow canals and is less efficient for wider canals.

Before discussing experimental results of canal gap mapping, the utility of the theoretical model introduced above should be discussed in more detail. Canal gaps in peat swamp forest show up more prominently in radar images when they are oriented more closely in azimuth direction and when they are wider. The theoretical model can be used to quantify these relationships; moreover, it can be used to predict the effect of forest structural parameters and incidence angle on these relationships.

This can be done by introducing the parameter "contrast", which simply is the sum of the absolute radar backscatter change (in dB) of the disturbance in the forest canopy caused by the canal gap, as shown in Figure 6. This sum is taken over pixels of a single row (i.e., east–west direction) matching the canal disturbance section. Higher contrast values can be related to higher visibility of canals gaps in the radar image. Higher contrast values are found for canals gaps wider than 10 m in combination with a canal orientation smaller than 75 degrees from azimuth direction (see Figure 9).
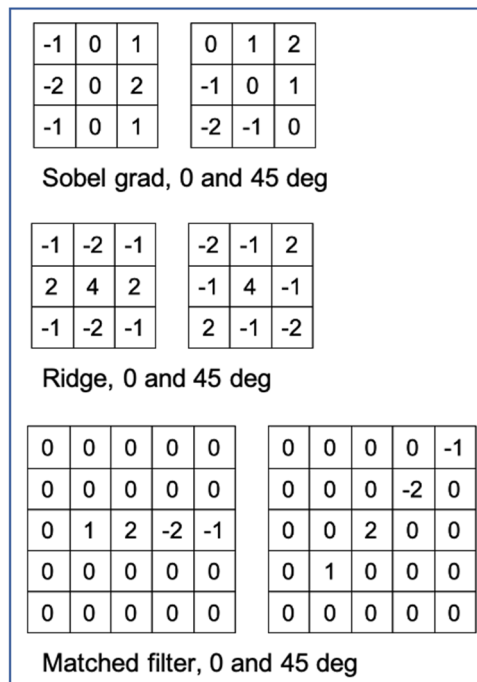
Figure 8. Sobel gradient, ridge and matched filters used for canal gap detection. Only the 0° (east–west) and 45° orientations are shown.
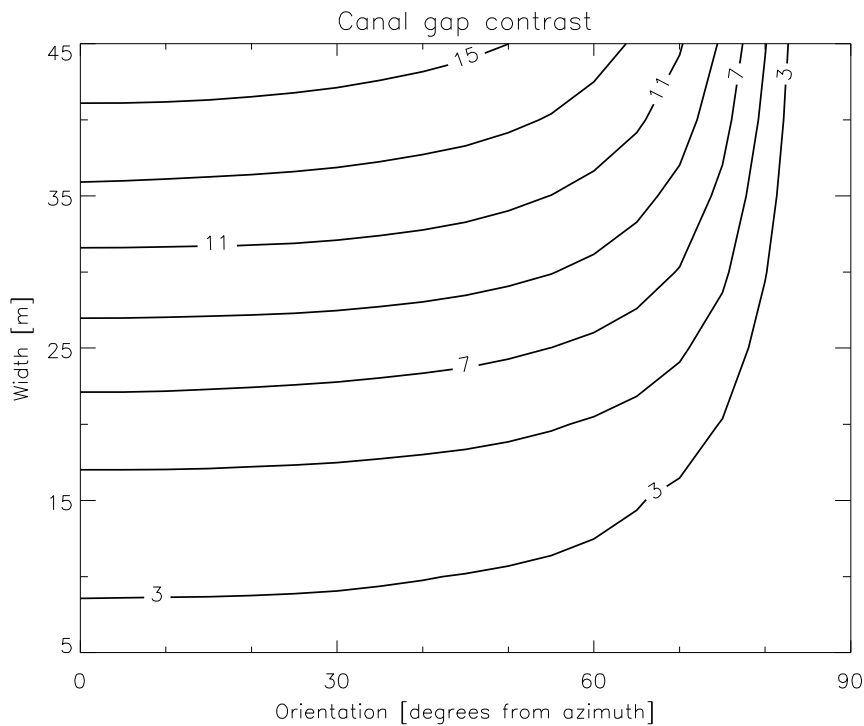
Figure 9. Contour plot of modelled contrast (dB) as function of orientation (degrees from radar azimuth) and canal gap width (m).

Since the contrast parameter is independent from canal length, it also applies for gaps of very short canals, which resemble gaps caused by selective logging. These small canopy gaps, or forest degradation gaps, are usually not elongated. Therefore, it may be assumed that contrast values for small orientation angles apply. Furthermore, it can be noted that, for small angles, the ratio between contrast and gap width is almost constant when the gap width is above 20 m. The latter relation

can be computed by using the same model and depends on incidence angle and forest structure. In Figure 10, the relation between contrast and degradation gap width for a peat swamp forest at three incidence angles is shown. This example shows that lower incidence angles give higher contrast. Simulations also show that higher forest, in general, gives higher contrast. Therefore, when the right model is applied and contrast is not computed over a single gap section but over a certain fixed area (e.g., 10 × 10 pixels), then the averaged contrast can be related to the fraction of the forest canopy lost because of degradation. Examples for quantification of degradation are discussed in Section 3.3.
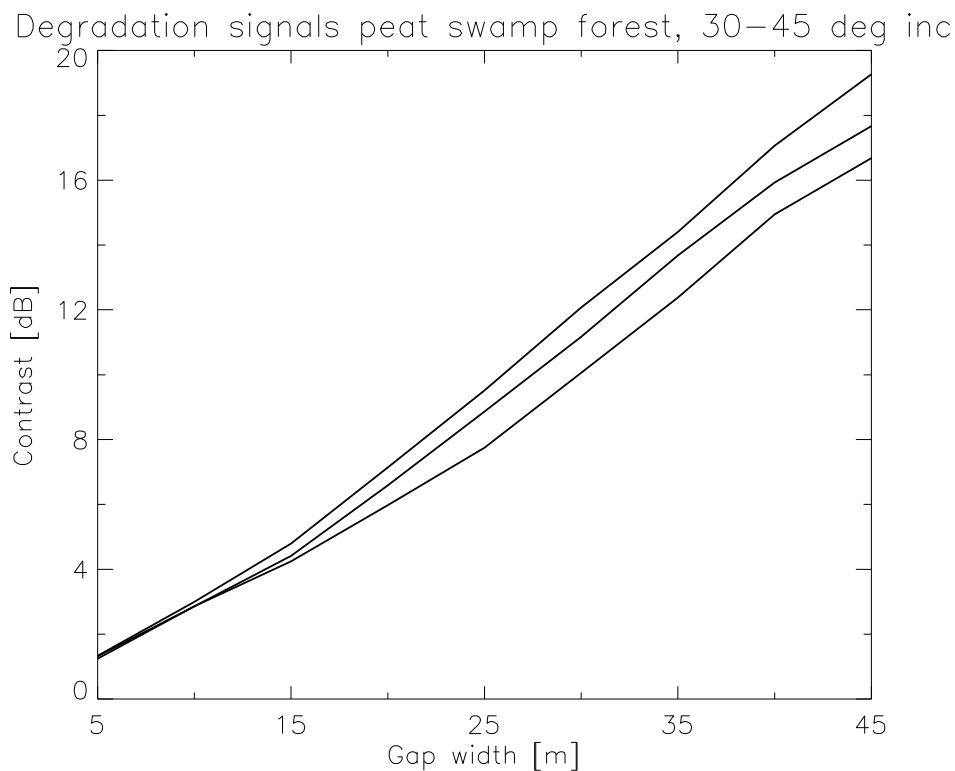
Figure 10. Modelled contrast (dB) as a function of canal gap width (m) for a peat swamp forest in Central Kalimantan for three radar incidence angles. Steeper incidence angles yield higher contrast: 30.0 degrees (top), 37.6 degrees (middle), and 45.0 degrees (bottom).

3. Results

3.1. Results for Canal Gap Detection

The Sentinel-1 NRT canal maps were validated by using results of visual interpretation of SPOT-6/7 images as reference. For each canal visible, the length, width, and orientation were determined. The detection rate was studied by comparing the lengths of these canals with the corresponding lengths in the Sentinel-1 map. This was done as a function of canal width and orientation. The false-alarm rate was studied by evaluating Sentinel-1 canal detections not present in the initial reference dataset. A large fraction of the initial reference map for 8 August 2017 is shown in Figure 11a, while, in Figure 11b, the corresponding Sentinel-1 NRT canal map for 7 August 2017 is shown.

The overall detection rate is 85.5%, i.e., 9.3 km of canal length is missed out of a total 64.2 km. Tables 3–5 divide this result over several width and orientation classes. Only for the smallest width class (5–10 m range, Table 3) and the orientation two classes closest to the range direction (more than 80 degrees from azimuth direction, Table 4), the accuracy drops below 50%. Table 5 combines these 2 classes showing that for small canals (smaller than 20 m) in radar look direction (within ±15 degrees from range direction) the accuracy drops to 27.3%. In all other cases, the accuracy is much higher, which is in agreement with the simulated result presented in Figure 9.

(a)

(b)

(c)
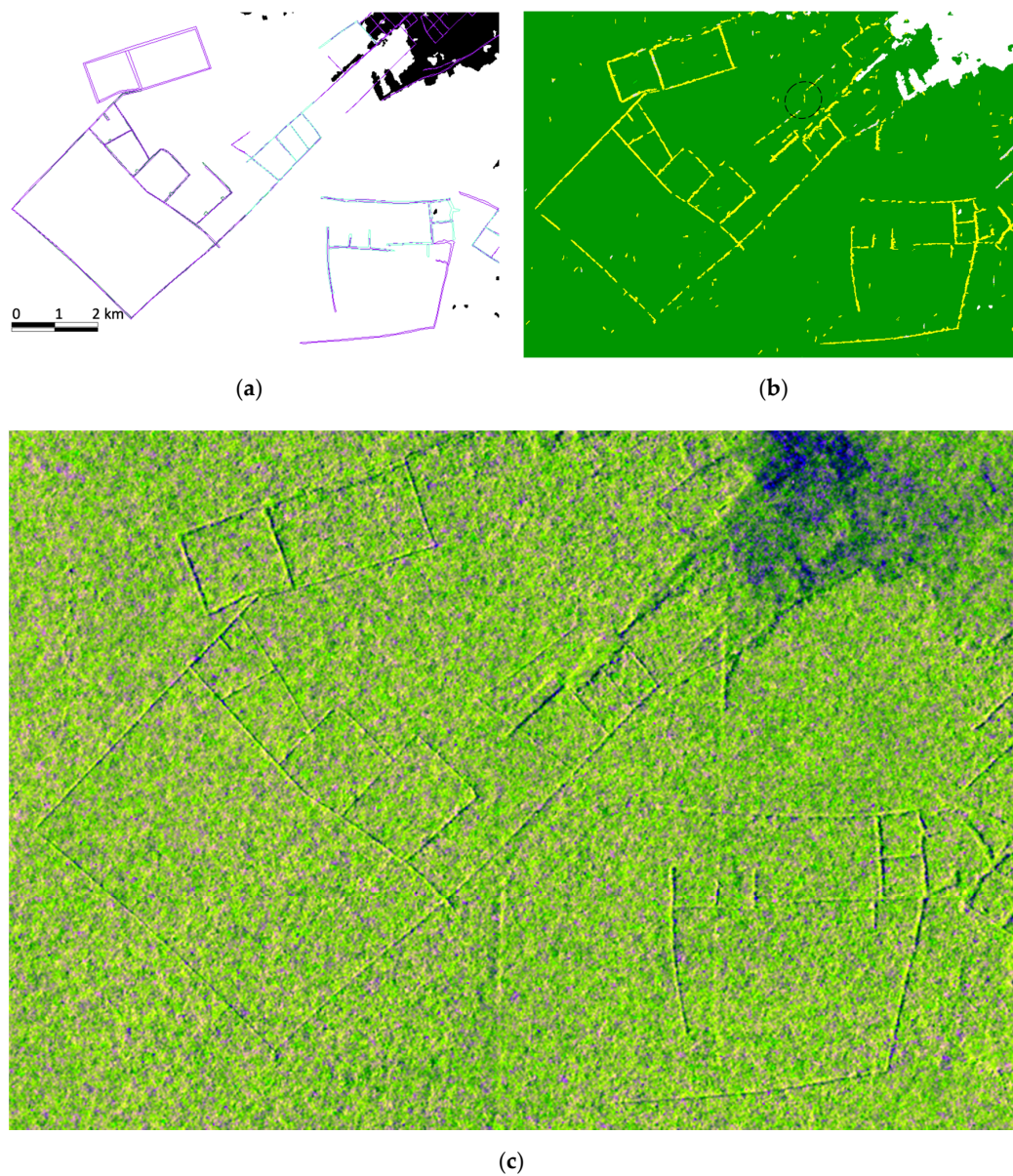
Figure 11. (**a**) Reference data from SPOT-6/7 20170908; (**b**) detail Sentinel-1 (S1) NRT canal map 20170907, 11.6 km × 7.9 km; (**c**) corresponding S1 radar image 20170907. (Standard color scale: see caption for Figure 2.)

Table 3. Detection rate based on canal width.

Width (m)	Length (m)	Correct (%)
5–10	1559	47.4
10–15	15,634	77.8
15–20	13,462	91.3
20–25	7938	84.1
25–30	9351	99.9
30–35	3859	70.7
35–40	5838	84.4
40–45	2511	92.4
45–50	2861	87.8
>50	1186	100.0
Total	64,197	85.5

Table 4. Detection rate based on look direction.

Azimuth	Length (m)	Correct (%)
0–5	2283	97.8
5–10	152	100.0
10–15	720	100.0
15–20	3555	99.7
20–25	1511	99.3
25–30	1119	98.7
30–35	12,283	95.0
35–40	4470	83.2
40–45	3255	94.8
45–50	2562	83.2
50–55	2827	95.6
55–60	6883	79.3
60–65	7317	81.4
65–70	903	84.5
70–75	6048	81.1
75–80	6610	68.4
80–85	1422	45.2
85–90	275	27.3
Total	64,197	85.5

Table 5. Detection rate for wide and narrow canals, oriented in look direction or other direction. Here, wide means >20 m; in look direction means within ±15 degrees from range direction.

Combination Classes	Length (m)	Correct (%)
Wide, not in look direction	25,510	96.2
Wide, in look direction	8032	64.3
Narrow, not in look direction	30,379	82.7
Narrow, in look direction	275	27.3
Total	64,197	85.5

Sentinel-1 canal detections not present in the initial reference set could be divided in two different categories. The first category consists of true canal gap segments very poorly visible in the SPOT images. These canal gaps are often narrow and often show regrowth. An example is given in Figure 12. Once these canals are recognized in SPOT images, aided by the Sentinel-1 maps, additional visual interpretation is possible. In this study, 7.3 km of additional canal gaps could be found in the SPOT data, of which 4.6 km (or 62.7%) was actually already mapped by Sentinel-1. This includes three canals smaller than 10 m, all oriented at 55 degrees from azimuth direction: (1) 9.7 m width, 114 m length, and 100.0% detected; (2) 8.1 m width, 340 m length, and 100.0% detected; and (3) 6.5 m width, 348 m length, and 48.3% detected. The second category consists of small canal gap segments in the NRT map which are not visible in the SPOT images, even after careful re-evaluation. While a part of these false-alarm detections may constitute true false alarms, another part may be true detections (or "false false" alarms) not visible in the SPOT image, for example, related to small canopy gaps caused by illegal selective logging. This notion is based on an evaluation of a time-series of canal gap maps. For example, in the 7 August 2017 NRT canal gap [NRT(N = 0)] map, the false-alarm rate is 9.5%. However, in subsequent maps, an increasing number of these false alarms disappear. Therefore, these false alarms may be related to noise effects and could be regarded as true false alarms. After approximately two months of persistent false alarm detections remain. These persistent false alarm detections, unlike the non-persistent false alarm detections, are not located at random, but are located near canals and rivers or forest edges. These places are much more accessible and prone to illegal logging activities. Thus, the false alarm rate of 9.5%, after approximately two months, may be divided in a non-persistent false alarm rate of 3.9% and a non-verifiable false alarm rate of 5.6%, which may relate, to a large extent, to true disturbances such as illegal logging.

Figure 12. Location of canals hardly visible in SPOT-6/7 corresponding with the detections by Sentinel-1 in the black ellipse of Figure 11b. The inset located in the upper-left shows the corresponding area of the Sentinel-1 NRT canal gap map.

3.2. Results NRT Deforestation Monitoring

Sentinel-1 NRT deforestation maps were validated in Borneo and Brazil, using a careful visual interpretation of all available Sentinel-2 images and Google Earth. The result is an optical reference set of image segments labelled either as completely forested or completely deforested. These optical segments are compared with individual pixels in the radar maps. Before discussing the results of this validation, it may be insightful to compare an S1 radar NRT deforestation map with an S2 deforestation map, where all pixels of the S2 map which have at least a small bare soil fraction in at least one of the images used for validation are marked as deforested (Figure 13). This map clearly shows large agreement between optical and radar data for deforested areas. However, for forest areas recovering from fire, newly degraded areas, and narrow linear gaps (new roads and canals), large fractions are missing in the S2 map.

Table 6. Overview Sentinel-1 NRT map series and Sentinel-2 reference data series. For Brazil, two Sentinel-2 series were used.

| Series	Number	Period
Indonesia S1	91	20150930–20190804
Indonesia S2	157	20170119–20191120
Brazil S1	81	20170108–20191001
Brazil S2	63	20170616–20191029
Brazil S2	56	20180524–20191130
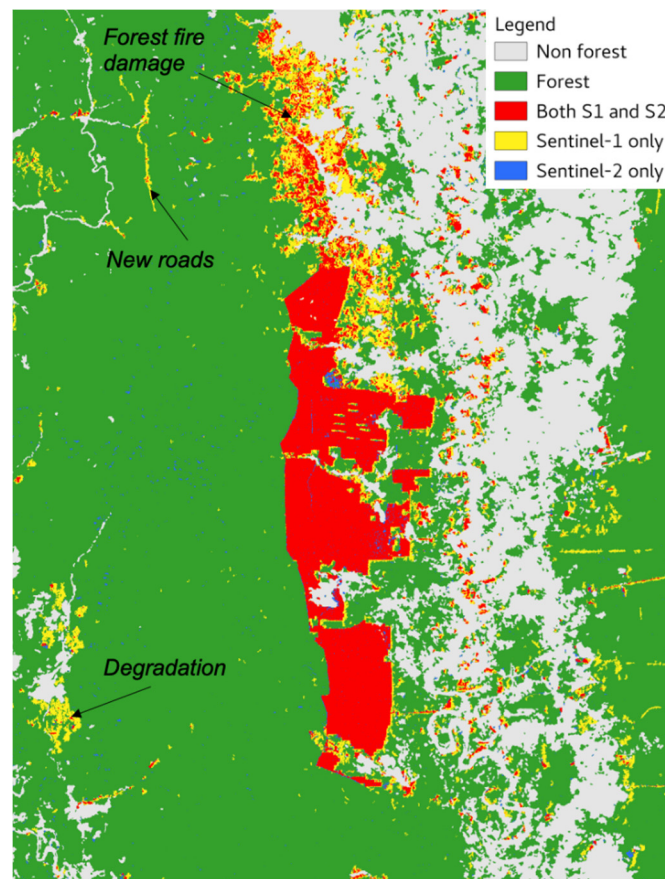
Figure 13. A 30 km × 40 km section of an S1 deforestation map of August 2019 is compared with a Sentinel-2 (S2) reference map for an oil palm development area on shallow peat in Central Kalimantan. The S2 reference map shows the cumulative detection (for all available S2 images, see Table 6) of pixels with a bare soil fraction. For large-scale deforestation, there is a large agreement (red). In other areas, such as forests recovering from fire damage and degraded forest, the S2 reference misses large areas (yellow). The same is true for new road and canal gaps.

Results of (quantitative validation at radar pixel level) can be shown in charts, as in Figure 14a. This example is the aggregated result for three representative landscapes in Central Kalimantan with a total area of 194,235 ha, and with major deforestation events in the Sentinel-1 observation period. Within these landscapes, all areas interpreted as deforested in the Sentinel-2 images while being classified as forest in the 2015 baseline map were evaluated. An overview of the S1 NRT maps and the S2 images used for validation are given in Table 6. In the chart of Figure 14, the transition in time from forest to non-forest is visible in terms of the classes used for validation. Only the classes MD (orange) and FA (red) represent errors. In the vertical direction the relative strength of the errors is visible and in the horizontal direction the duration of the errors.

The FAR (Equation (1)), in this example (Figure 14a), is very low, and is discussed later. The MDR (Equation (2)) is sometimes substantial and varies over time. For example, on 30 April 2019, at a 90% confidence level, the MDR has a value of 18.6% ± 1.0%, while, on 17 June 2019, the MDR is 1.9% ± 1.1%. This variation can be explained partly in methodological terms and partly in physical terms. The presented result relates to the default NRT(N = 1) system (see Section 2.4). This means detected deforestation is only (or mostly, depending on system settings) mapped when it can be confirmed by the next radar image. This is often not the case, as is illustrated by the time-series of radar images in Figure 15. This series of eight consecutive radar images, covering an oil palm plantation development area on shallow peat, clearly demonstrates the backscatter contrast between forest and new clear-cut can go up and down. This may be explained, physically, by the relatively large soil

roughness in combination with changes in soil moisture. The same phenomenon is illustrated in segment-averaged temporal backscatter signals for VH, VV, and VH–VV ratio for the same area in Figure 16a. The VH and VV signals jointly go up and down, and deforestation is detected at the first moment it stays down. However, the VH–VV ratio stays low from the moment the VH and VV signals go down for the first time. The lowered VH–VV ratio is a sign of vegetation loss and the fluctuation of the VV and VH are signs of soil moisture fluctuations. High levels of soil moisture and large soil roughness in combination with the NRT(N = 1) methodological rules explain the delay in deforestation detection in this shallow peat landscape. It could also be noted that, on average, the delays are larger in the deep peat landscape and absent in the dry forest landscape. This may be related to other soil roughness and/or soil drainage conditions.
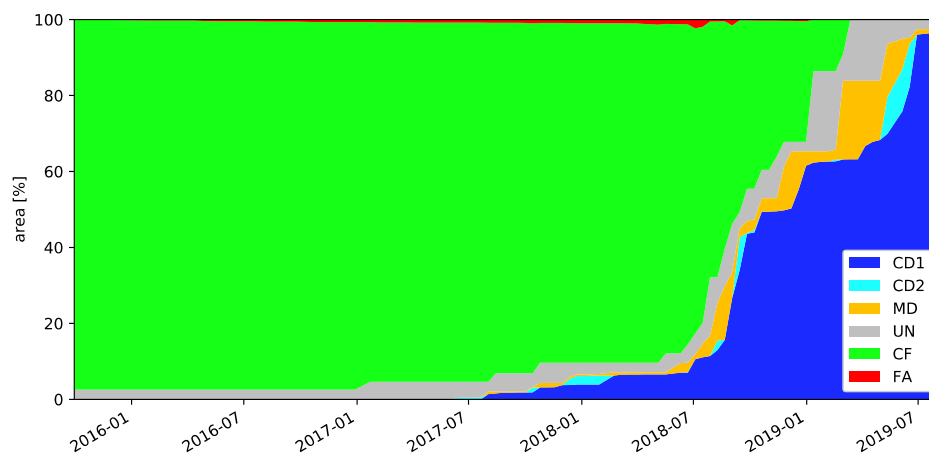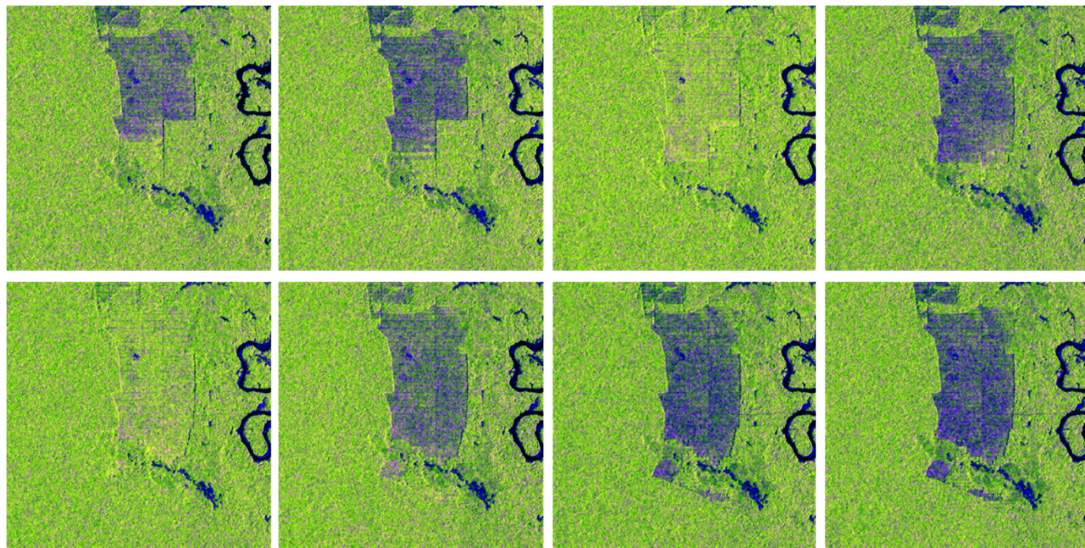

(**a**)
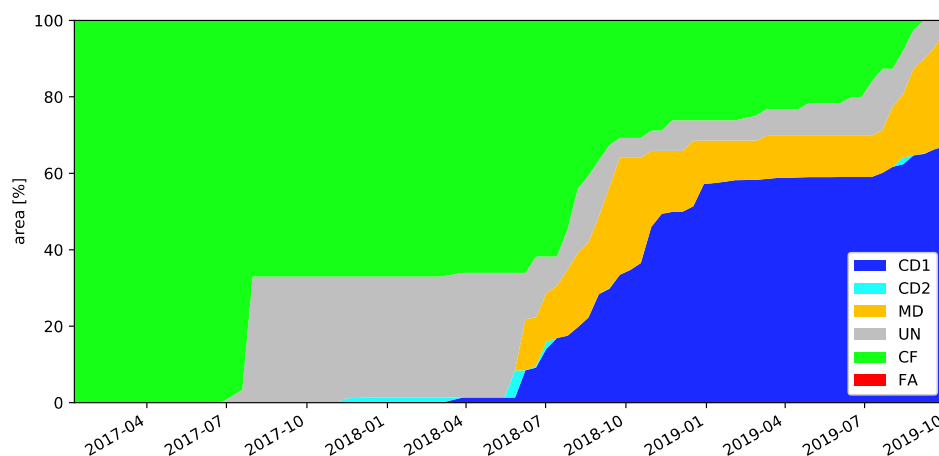
(**b**)

Figure 14. (**a**) Aggregated validation results for three representative landscapes in Central Kalimantan for the period September 2015 until August 2019. (**b**) Aggregated validation results for representative landscapes in Pará, Brazil, for the period January 2017 until September 2019.

Figure 15. Eight successive radar observations at a 12-day interval for the period 20180704–20180926 (from top left to bottom right). Area: 10 km × 10 km. Location: Central Kalimantan. (Standard color scale: see caption Figure 2.)

(**a**)

(**b**)

(**c**)
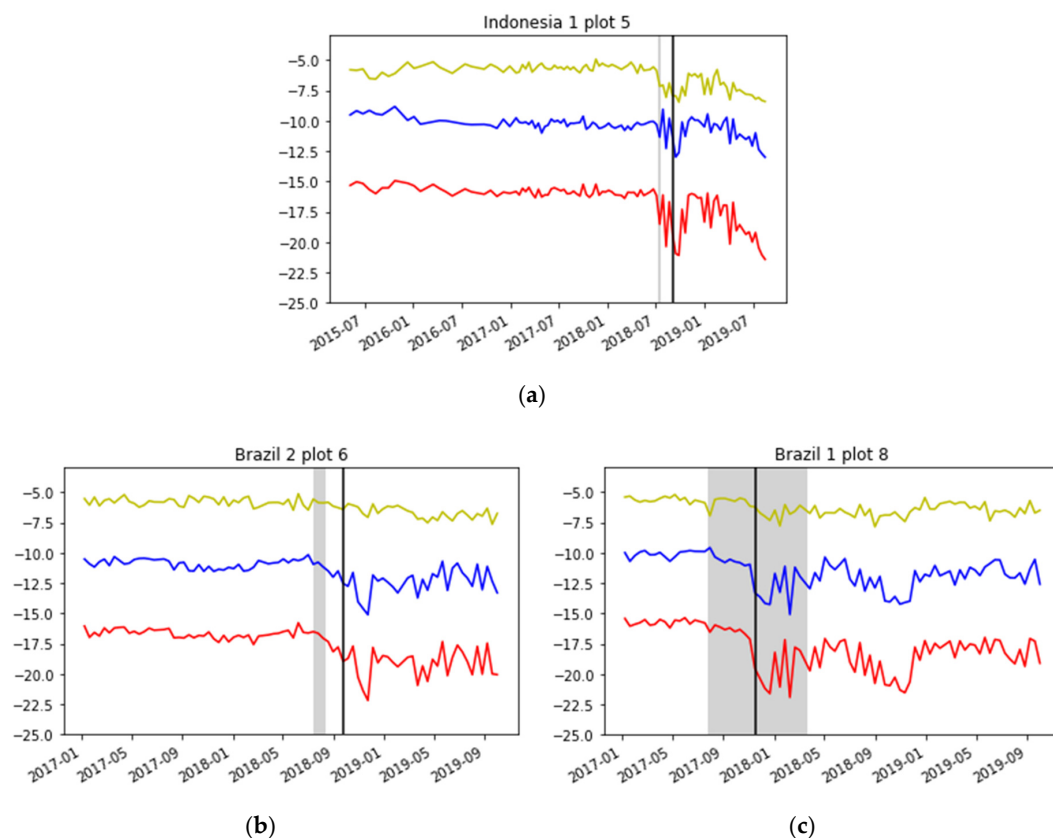
Figure 16. (**a**) Temporal radar signature for an area located in Figure 15. VH-polarization (red), VV-(blue), VH/VV-polarization (red). The black line shows the time of detection for the NRT (N = 1) system, and the gray line is the reference time following from visual interpretation of Sentinel-2. (**b**) Temporal radar signature for an area in Brazil where, after the first indication of deforestation on S2, radar backscatter decreases slowly. This causes a delayed detection by an NRT (N = 1) system. (**c**) Temporal radar signature for an area in Brazil with much more cloud cover. In this case, Sentinel-2 data can only show that deforestation occurred within the gray interval.

These results can be compared with a representative landscape north of the Amazon River in the State of Pará, Brazil, with a total area of 57,792 ha, as shown in Figure 14b. This landscape is characterized with small-scale deforestation, often of the slash-and-burn type. Deforestation is often preceded by severe degradation and sometimes changed in low secondary vegetation without ever passing through a bare soil state. In the latter case, the change in averaged radar backscatter is low and deforestation is only detected well along the near range forest edges as radar shadow and partly as degradation (see Section 3.3). This explains the aggregated validation results for the Brazil landscape shown in Figure 14b. Like in Indonesia, the FAR is very low and the MDR is sometimes substantial and varies over time. The MDR may be split for MD which is followed by correct detections within a short period and persistent MD related to areas that never experience a stage without substantial vegetation cover. For example, at 10 January 2019, at a 90% confidence level, the MDR is 17.0% ± 1.6%, which can be split into a temporary part of 3.3% ± 1.5% and a persistent part of 13.8% ± 1.4%. These numbers do not change much until 21 July 2019, when significant temporary MD cases start to occur. Figure 16b illustrates the gradual deforestation process typical for this landscape. The backscatter decreases over a period of several months before deforestation is detected. Gradual deforestation may partly explain the delay in deforestation detection, which is unlike the situation in Indonesia where delayed detection may be better explained by high levels of soil moisture (mainly on peat).

In summary, it can be concluded that the FA rate is very low (because of selected user settings) and the MD rate can be significant and varies because of delays in detection; however, the MD error is not permanent. The detection delay is a typical feature of the NRT(N = 1) system. Such delays are absent in the NRT(N = 0) system at the expense of a higher FA rate (for example caused by heavy rain cells). In an NRT(N ≥ 2) system, the delays are much shorter at the expense of having less timely maps. This may illustrate the importance of proper user settings or adopting a more complex system with multiple sets of user settings.

Opposed to detection delays in radar data, there are also detection delays in optical data. The class CD2 shows radar detection prior to the first available next optical image. However, there are many more cases where radar detection precedes optical detection. In the validation procedure, these cases are present in the class unknown (UN), but these cases cannot be validated, by definition, by optical data. An example is given in Figure 16c. Because of cloud cover, the optical data can only be used to show the deforestation occurs in the period August 2017 until April 2018. The radar detection is in the middle of this period, where a significant drop in the radar backscatter occurs. In cases where validation could be done, a drop of such a magnitude leads to a correct deforestation detection. An evaluation of the radar signatures of all test areas reveals that, for the Brazilian landscape, in more than 20% of the cases, the radar detection precedes the optical detection by at least two months and up to 11 months. For the Indonesian landscapes, all relatively close to the coast, where there is less cloud cover, the radar detection precedes the optical detection in approximately 10% of the cases by at least two months and up to eight months.

In the presented examples (Figure 14a,b), the FAR is always very low. This result should be interpreted as follows. FAR and MDR are dependent. The selected settings of the algorithm used for this example favor a low FAR at the expense of a relatively high MDR. The results shown are at pixel level, while the optical reference data, based on visual interpretation, are at segment level. Within the segment a very small fraction of pixels may relate to small scale deforestation such as road development prior to deforestation, or small remnant patches of trees after deforestation. These fractions cause small FAR and MDR errors.

3.3. Results NRT Degradation Monitoring

3.3.1. Brazilian Study Site

Since the theoretical model introduced in Section 2.5 applies equally well for gaps of very short canals, which resemble gaps caused by selective logging, it can be used to quantify degradation.

When the right model parameters are applied and contrast is computed over a certain fixed area (e.g., 10 × 10 pixels), then the averaged contrast can be related to the fraction of the forest canopy lost resulting from degradation (e.g., Figure 10). A mapping example for an active section in a Brazilian timber concession area is shown in Figure 17.
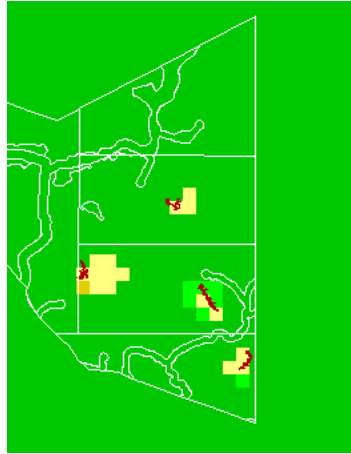

Figure 17. A section of a Sentinel-1 radar derived map showing deforestation at pixel level (red) and quantitative degradation for 150 m × 150 m blocks in a timber concession area (demarcated with white lines). Area: 4 × 5 km. Degradation classes expressed in canopy loss fraction: <20% (light green), 20–30% (yellow), 30–40% (tan), and >40% (pink). Almeirim, Brazil, February 2018.

Radar is a suitable instrument to quantify degradation. Unlike optical data, which detect degradation mainly by the signal fraction from the bare soil, the radar detects degradation by signals from gaps in the canopy, even when the understory still covers the soil. Therefore, the radar signal is very persistent (gaps in the upper canopy do not fill up fast), while the optical signal is visible for a short time window only (secondary regrowth on bare soil appears fast). The latter is even more troublesome when cloud cover is frequent. This is illustrated well by the example given in Figure 18. Here, for a selective logging concession area in Brazil a comparison is made between the Sentinel-1 radar and Sentinel-2 optical results. The solid line shows the total forest canopy fraction loss for each radar observation as a function of time. For optical data, such a result is not feasible because of cloud cover; instead, the accumulated detections can be shown (dotted line with diamonds). This accumulated result sums all detections, even when they are not visible anymore because of regrowth or cloud cover. It can also be noted that in this period where 81 radar observations were made only 12 partly cloud-free optical images (diamonds) are available (see Table 7). From the comparison, it is clear that most degradation in the wet season (December–May) is not detected by the optical system. Obviously, optical data have severe limitations to detect degradation and, thus, are less suitable for the validation of radar degradation maps. An alternative is the use of high-resolution radar data, such as TerraSAR-X, which are used to map selective logging at the level of individual canopy trees [20]. Results for the wet season, in January–February 2018, show a clear correspondence in time and location of degradation. The 85 trees logged in this period (mapped by TerraSAR-X) compare with an effective forest canopy fraction loss of 4.5 ha (mapped by Sentinel-1). This would relate to an average loss of ±500 m^2 per logged canopy tree.
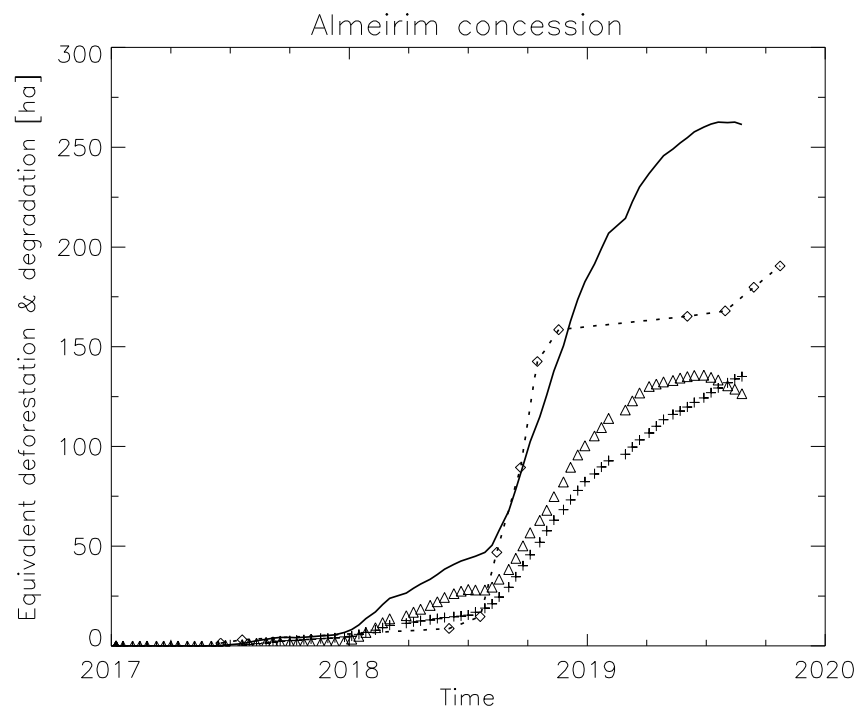
(a)
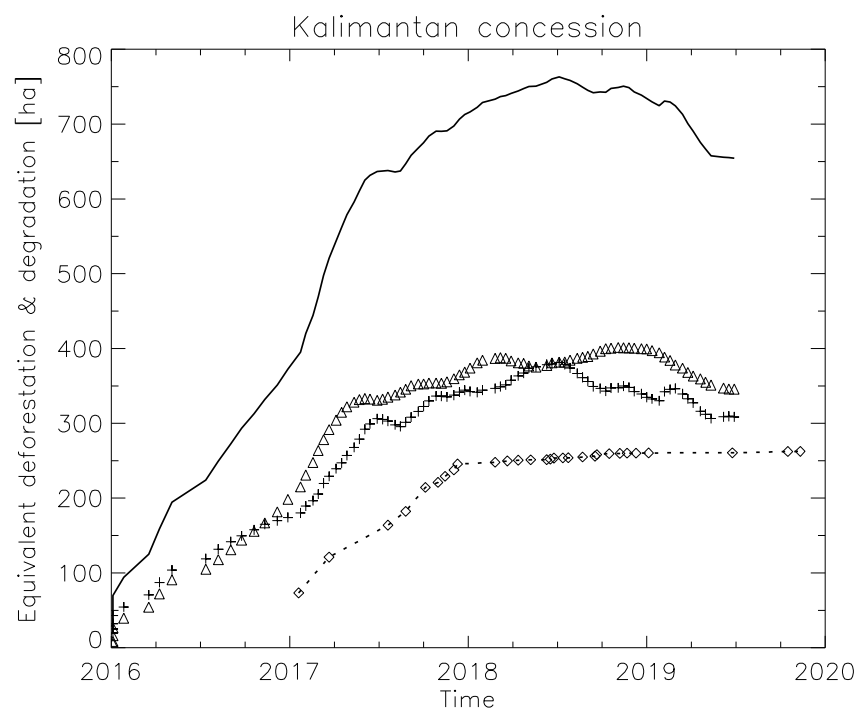
(b)

Figure 18. (**a**) Results of degradation mapping for a selective logging timber concession in Almeirim, Brazil. Total forest canopy fraction loss as a function of time for radar (solid line), which is the sum of the fraction related to canopy gaps (triangles) and the fraction related to timber trails (plusses). For optical data, the accumulated detections are shown (dotted line with diamonds). The symbols indicate the time of observation (scaled between January 2017 and December 2020). (**b**) As Figure 18a, for a timber concession in Central Kalimantan.

Table 7. Overview Sentinel-1 NRT map series and Sentinel-2 and TerraSAR-X (3 m single-pol stripmap) reference data series.

| Series	Number	Period
Indonesia S1	88	20160104–20190804
Indonesia S2	29	20170119–20191110
Brazil S1	81	20170108–20191001
Brazil S2	12	20170616–20191024
Brazil TerraSAR-X	3	20171203–20180207

3.3.2. Indonesian Study Site

A second example is given for a timber concession located in Central Kalimantan on undulating terrain (250–1100 m altitude). For this area Sentinel-1 degradation maps have been made from January 2016 onward. For Sentinel-2 29 partly clouded images are available since January 2017. These images were used to delineate all disturbance through careful visual interpretation. Results (Figure 18b) are shown in a similar way, as was done for the Brazilian site. The study area (shown in Figures 19 and 20) is 8000 ha large. The radar shows that an equivalent area of approximately 400 ha is lost in the year 2016 and another 300 ha in 2017. The first Sentinel-2 image shows a loss of only ±80 ha. This is partly explained by partial cloud cover; however, almost all of the 2016 losses detected by radar were not detected, either, in the following 28 Sentinel-2 images. The accumulated losses visible in the optical data increase until ±280 ha, while the instantaneous losses mapped by radar peaks at ±750 ha in mid-2018, followed by a slight decrease, which may be attributed to regrowth.

The evaluation of the radar and optical maps shown in Figure 19a–e and the corresponding radar images (Figure 20) of this area allows for a more detailed discussion. This is done for three moments in time: one of the first radar degradation maps (August 2016: Figure 19a); the first optical reference map and the associated radar degradation map (January 2017; Figure 19b,c); and the optical reference and radar map around the end of the logging operation (December 2017; Figure 19d,e). The radar images coincide with the August 2016 radar map (Figure 20a) and the December 2017 radar map (Figure 20b). A visual comparison of these two radar images clearly shows a change in the road network but no clear signs (i.e., backscatter level or textural change) of degradation. Nevertheless, degradation can be mapped based on model-based calculations using the changes in the patterns that constitute the texture (Figure 19a,c,e). In the first Sentinel-2 reference map (Figure 19b) the main road network is well visible as well as some small canopy gaps. These gaps correspond almost completely with the area of current activity, while most of the gaps visible in the August 2016 radar map, five months earlier, are not visible. The December 2017 Sentinel-2 reference image shows the accumulated visibility of roads and gaps. New roads and gaps show up at the same location as in the radar map. However, in general, there are two qualitative differences. The first, as discussed above, radar detects more forest loss related to gaps. Secondly, the radar maps show less roads than the optical reference image, for which there are two causes. The first cause is that the radar maps only show change with respect to the baseline. Therefore, existing and stable road gaps do not show up while in the optical reference image they are still mapped. One clear example is the gap caused by a river visible in the upper left corner of Figures 19d and 20. The second cause is the use of an MMU of 1 ha for mapping of clear-cut in this forest type. Since narrow roads may break in multiple smaller segments, some smaller than the MMU, these missed sections may be mapped as degradation instead. The same is true for wider roads oriented in the radar range direction, as discussed in Section 3.1, which is visible, for example, in the top-right of Figure 19d,e. It is noted that, for the calculation of the total equivalent area of forest loss (as shown in Figure 18a,b), it does not matter whether a small narrow road section is classified as deforestation or as degradation.

(**a**)

(**b**)

(**c**)

(**d**)

(**e**)
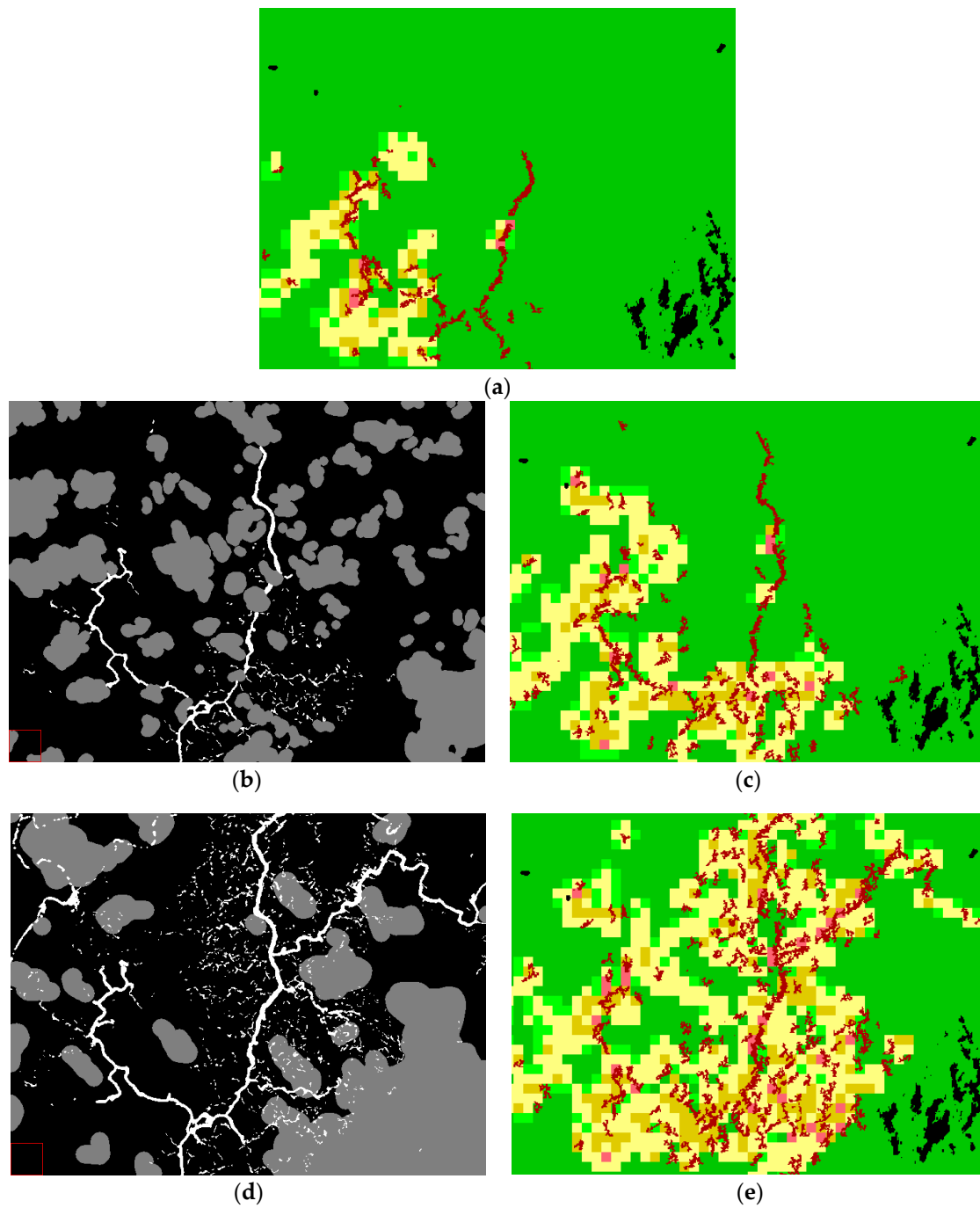
Figure 19. (**a**) S1 degradation map 20160807. Detail of a timber concession area in Central Kalimantan. Area: 7.3 × 5.6 km. (Legend: see caption Figure 17). (**b**) S2 reference map 20170119 and (**c**) corresponding S1 degradation map 20170122. In the S2 reference map, cloud cover in the last available image is shown in gray, and the accumulated visibility of roads and gaps is shown in white. (**d**) S2 reference map 20171210 and (**e**) corresponding S1 degradation map 20171212.
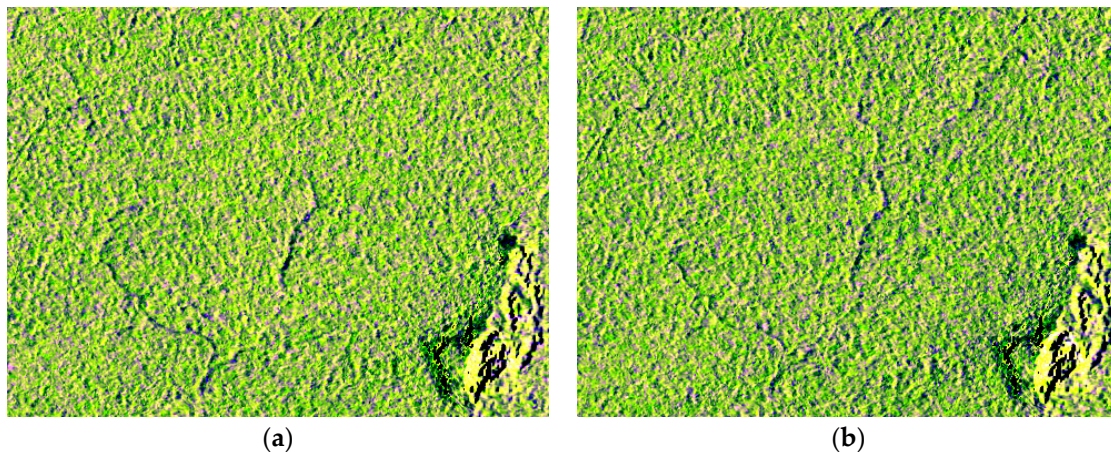
Figure 20. (**a**) S1 radar image 20160807 and (**b**) S1 radar image 20171212. Same area as in Figure 19. (Standard color scale: see caption Figure 2.)

4. Discussion

4.1. System and Disturbance Model

The Sentinel-1 NRT radar monitoring system is an automated system based on interferometric preprocessing and time-series analysis of small image segments, linear features, and small-scale disturbances. This results in a system that can accurately map different phenomena simultaneously, such as deforestation (clear-cut and fire scars), degradation, selective logging impact, and new narrow canals in peat swamp forest. Radar imaging of canal gaps and the canal-gap-detection mapping results were shown to be in agreement with a physical-interaction model. Small gaps caused by selective logging are too small to be detected individually; however, the same theoretical model (that describes canal gaps) can be used to quantify the canopy disturbance in a statistical sense. Therefore, change mapping is done in three fundamentally different ways. Deforestation is detected by using segment-based time-series analysis and uses a decrease of backscatter as an indicator of deforestation. Canal-gap detection is based on time-series analysis of linear features, using edge, line, and matched filters. Degradation is quantified by using a time-series analysis of textural change based on a physical model. These three approaches are not completely independent, not from a data processing point-of-view, nor from a forest-change-interpretation point-of-view.

Several examples of interdependency can be given. For deforestation mapping in peat swamp forests an MMU of 15 pixels (0.3 ha) applies. This means that wide canal gaps are often mapped as (a row of individual) segments. The same canal gaps show up in the canal gap maps as linear features. Of course, the dedicated canal gap product shows more canals, including some very narrow ones which are hardly visible in SPOT-6/7 data. Very small deforestation segments or very short canal gap detections are often part of degradation areas. At the Brazil test sites some areas of deforestation, the ones that gradually change from forest to low secondary forest without going through a bare soil stage, are not detected with the deforestation mapping approach. However, the near range edges of such areas are still visible as elongated segments, and parts of these areas are detected as degraded. Using such interdependencies explicitly may contribute to a better interpretation of ongoing forest-change processes.

4.2. Deforestation

Deforestation detection success is evaluated by using results of a careful visual interpretation of Sentinel-2 time-series as a reference. These results are independent of any issues related to baseline class definitions and timing. In summary, for the Central Kalimantan landscapes, it is shown that the false alarm rate (FAR) is very low (less than 1%) and the missed detection rate (MDR) varies between

18.6% ± 1.0% and 1.9% ± 1.1% (90% confidence level). However, results also depend on user settings. FAR and MDR are interchangeable. Settings were selected to favor a low FAR at the expense of a slightly higher MDR. Another compromise to be made is between overall accuracy and timeliness. In other words, the faster the maps should be made available after radar observation, the lower the accuracy. Settings were selected to favor a relatively fast system, which results in significant detection delays in the map time-series. It was found that peatlands are a typical case where detection delays up to two months occur which are caused by the combination of rough soil surface and high soil moisture. This is causing the high MDR, but these missed detections are only temporary, not permanent. Other settings could decrease such delays to a few weeks. These delays were not found outside the peat areas or in the Amazon. Because of cloud cover, radar can be much faster than optical systems, but this cannot be validated by optical systems. It was found that radar very often detects deforestation two months and up to 10 months faster than optical systems.

4.3. Canal Gap Detection

Results of visual interpretation of SPOT-6/7 images were used as reference. The overall detection rate is 85.5%; however, results strongly depend on canal gap orientation and, to a lesser extent, on canal gap width. Only for the smallest width class (5–10 m range) or for orientations of more than 80 degrees from azimuth direction, the accuracy drops below 50%. In total, 9.3 km of canal length was missed out of a total 64.2 km. Sentinel-1 canal gap detections which were not present in the initial reference set could be divided in two different categories. The first category consists of true canal gap segments very poorly visible in the SPOT images. These canal gaps are often narrow and often show regrowth. Once these canals are recognized in SPOT images, aided by the Sentinel-1 maps, additional visual interpretation is possible. In this study, 7.3 km of additional canal gaps could be found in the SPOT data. The second category consists of small canal gap segments in the NRT map which are not visible in the SPOT images, even after careful re-evaluation. A part of these false alarms is persistent while others disappear within two months. These persistent false-alarm detections, unlike the non-persistent false-alarm detections, are not located at random, but are located near canals and rivers or forest edges. These places are much more accessible and prone to illegal logging activities. Therefore, the false alarm rate of 9.5%, after approximately two months, could be divided into a non-persistent false alarm rate of 3.9% and a non-verifiable false alarm rate of 5.6%, which may relate to a large extent to true disturbances, such as illegal logging.

4.4. Degradation

Like for deforestation, degradation detection success is evaluated using results of a careful visual interpretation of Sentinel-2 time-series as a reference. Radar is a suitable instrument to quantify degradation. Unlike optical data, which detect degradation mainly by the signal fraction from the bare soil, the radar detects degradation by signals from gaps in the canopy, even when the understory still covers the soil. Therefore, the radar signal is very persistent (gaps in the upper canopy do not fill up fast), while the optical signal is visible for a short time window only (secondary regrowth on bare soil appears fast). The latter is even more troublesome when cloud cover is frequent. Validation is difficult using optical data since degradation is detected in a fundamentally different way and a lot of degradation is missed. Nevertheless, results are spatiotemporally consistent. It may be much better to use TerraSAR-X for validation of degradation, notably for quantitative validation. The result presented here, for Brazil, is based on limited data only but provides high spatiotemporal, as well as quantitative, agreement.

4.5. Comparison with Other Approaches Based on C-Band

Other existing methods based on C-band [43–46], which focus either on deforestation monitoring or forest/non-forest mapping, can be compared with the deforestation results presented here. The method for deforestation detection presented in Reference [43] provides a similar accuracy level, however,

requires both ascending and descending data. These are not available for most tropical forests, nor will they become available in the near future. The method for deforestation detection based on interferometric coherency [46] is less accurate; however, it may provide useful additional information. The results of forest/non-forest classification presented in Reference [44] also seem less accurate when used for the purpose of deforestation monitoring. The comparison with other systems is difficult because the system presented in this paper uses C-band for the monitoring part and a combination of L-band, C-band, and optical data for the (baseline) classification part.

5. Conclusions

Like JJ-FAST, the automated Sentinel-1 system presented here can be used for wide-area NRT forest-change monitoring. Results are available two days after satellite overpass, with higher spatial and temporal resolution and a high accuracy for deforestation detection. Unlike JJ-FAST, it utilizes multiple approaches for change detection, to allow monitoring of finer scaled features, such as narrow linear elements (roads and canals) and low-intensity degradation (selective logging). However, these refinements require the availability of a good forest baseline and system tuning to optimize it for local conditions, as well as local user requirements. The Sentinel-1 system is not meant primarily as a single system for pan-tropical coverage, but as a system to be operated and customized by local operators at the national level.

Though C-band, in general, has a lower forest/non-forest contrast than L-band, the Sentinel-1 radar in IW mode provides a higher temporal and spatial resolution than the PALSAR-2 ScanSAR mode, which makes Sentinel-1 equally suitable for the purpose of forest-change monitoring. One of the novelties in this paper is the use of the Sentinel-1 phase information for very precise co-registration (Section 2.3), which allows for the detection of subtle changes.

Though tested for large areas in Indonesia and the Amazon, the validation requires more efforts, which should result in more refined local tuning. For example, a preliminary test for entire Borneo over the entire period revealed that there are still some deforested areas which were not detected but would have been detected with slightly different system settings. The quantitative estimation of degradation is difficult to validate with optical data. More work is needed, using extensive field data as reference, to calibrate the radar proxy for degradation and compare it with optical proxies.

Even though degradation information is still not yet properly calibrated and validated, several interesting applications emerge. For example, the result in Figure 17 suggests that selective logging is not too intensive and is absent in the protected buffer zones along the river. This information is already helpful for planning field inspections in remote areas, certification, and transparency. Another example is early warning. Low-impact changes, such as new narrow roads, degradation, and small clear-cut areas in remote places are the first indications of potential future threats of forest-cover change. This information is already successfully used as input for predictive modelling based on machine learning by the World Wide Fund for Nature for the development of their Early Warning System (EWS) to predict deforestation [29]. The data also support and could modernize conventional approaches based on hi-res optical data, to get more information out of these data, such as discussed above for the detection of narrow canal gaps in SPOT-6/7 data. Alternatively, hi-res optical data acquisition, for example, after a long period of cloud cover, could be focused on areas where change actually has occurred. The availability of free Sentinel-1 radar data with a systematic and complete coverage is a great asset for future development of efficient wide-area forest-monitoring systems.

Author Contributions: Conceptualization, D.H., B.K., I.C., S.B., R.A. and O.R.; Formal analysis, D.H. and B.K.; Investigation, D.H., B.K. and R.A.; Methodology, D.H., B.K. and M.Q.; Resources, O.R.; Software, D.H. and B.K.; Validation, S.V. and R.A.; Visualization, B.K.; Writing—original draft, D.H.; Writing—review and editing, B.K., S.V., I.C., R.A. and O.R. All authors have read and agreed to the published version of the manuscript.

References

1. The State of the World's Forests 2020. Available online: http://www.fao.org/state-of-forests/en/ (accessed on 6 October 2020).
2. Walker, W.S.; Gorelik, S.R.; Baccini, A.; Aragon-Osejo, J.L.; Josse, C.; Meyer, C.; Macedo, M.N.; Augusto, C.; Rios, S.; Katan, T.; et al. The role of forest conversion, degradation, and disturbance in the carbon dynamics of Amazon indigenous territories and protected areas. *Proc. Natl. Acad. Sci. USA* **2020**, *117*, 3015–3025. [CrossRef] [PubMed]
3. Joosten, H.; Couwenberg, J. Peatlands and carbon. In *Assessment on Peatlands, Biodiversity and Climate Change*; Global Environment Centre: Kuala Lumpur, Malaysia & Wetlands International: Wageningen, The Netherlands, 2007; pp. 99–117.
4. Dargie, G.C.; Lewis, S.L.; Lawson, I.; Mitchard, E.T.A.; Page, S.E.; Bocko, Y.E.; Ifo, S.A. Age, extent and carbon storage of the central Congo Basin peatland complex. *Nat. Cell Biol.* **2017**, *542*, 86–90. [CrossRef] [PubMed]
5. Lähteenoja, O.; Page, S.E. High diversity of tropical peatland ecosystem types in the Pastaza-Marañón basin, Peruvian Amazonia. *J. Geophys. Res. Space Phys.* **2011**, *116*, 02025. [CrossRef]
6. Crump, J.; Avagyan, A.; Baker, E.; Barthelmes, A.; Velarde, C.; Dargie, G.; Guth, M.; Hergoualc'h, K.; Johnson, L.; Joosten, H.; et al. *Smoke on Water—Countering Global Threats from Peatland Loss and Degradation. A UNEP Rapid Response Assessment*; United Nations Environment Programme: Nairobi, Kenya and GRID-Arendal: Arendal, Norway, 2017; ISBN 978-82-7701-168-4.
7. IPCC. *2019 Refinement to the 2006 IPCC Guidelines for National Greenhouse Gas Inventories*; IPCC: Geneva, Switzerland, 2019.
8. Marziliano, P.A.; Veltri, A.; Menguzzato, G.; Pellicone, G.; Coletta, V. A comparative study between "default method" and "stock change method" of Good Practice Guidance for Land Use, Land-Use Change and Forestry (IPCC, 2003) to evaluate carbon stock changes in forest. *Secondo Congresso Internazionale di Selvicoltura Second Int. Congr. Silvic.* **2015**, 551–557. [CrossRef]
9. IPCC. *Definitions and Methodological Options to Inventory Emissions from Direct Human-Induced Degradation of Forests and Devegetation of Other Vegetation Types*; Institute for Global Environmental Strategies (IGES): Kanagawa, Japan, 2003; ISBN 4-88788-004-9.
10. GFOI. *Integrating Remote-Sensing and Ground-Based Observations for Estimation of Emissions and Removals of Greenhouse Gases in Forests: Methods and Guidance from the Global Forest Observations Initiative*; Group on Earth Observations: Geneva, Switzerland, 2014; ISBN 978-92-990047-4-6.
11. GOFC-GOLD. *A Sourcebook of Methods and Procedures for Monitoring and Reporting Anthropogenic Greenhouse Gas Emissions and Removals Associated with Deforestation, Gains and Losses of Carbon Stocks in Forests Remaining Forests, and Forestation*; GOFC-GOLD Report Version COP22-1; GOFC-GOLD Land Cover Project Office, Wageningen University: Wageningen, The Netherlands, 2016.
12. Souza, J.C.M.; Roberts, D.A.; Cochrane, M.A. Combining spectral and spatial information to map canopy damage from selective logging and forest fires. *Remote. Sens. Environ.* **2005**, *98*, 329–343. [CrossRef]
13. Asner, G.P.; Knapp, D.E.; Balaji, A.; Paez-Acosta, G. Automated mapping of tropical deforestation and forest degradation: CLASlite. *J. Appl. Remote. Sens.* **2009**, *3*, 033543. [CrossRef]
14. Franke, J.; Navratil, P.; Keuck, V.; Peterson, K.; Siegert, F. Monitoring Fire and Selective Logging Activities in Tropical Peat Swamp Forests. *IEEE J. Sel. Top. Appl. Earth Obs. Remote. Sens.* **2012**, *5*, 1811–1820. [CrossRef]
15. Potapov, P.; Hansen, M.; Kommareddy, I.; Kommareddy, A.; Turubanova, S.; Pickens, A.; Adusei, B.; Tyukavina, A.; Ying, Q. Kommareddy Landsat Analysis Ready Data for Global Land Cover and Land Cover Change Mapping. *Remote. Sens.* **2020**, *12*, 426. [CrossRef]
16. Hirschmugl, M.; Steinegger, M.; Gallaun, H.; Schardt, M. Mapping Forest Degradation due to Selective Logging by Means of Time Series Analysis: Case Studies in Central Africa. *Remote. Sens.* **2014**, *6*, 756–775. [CrossRef]
17. Hoekman, D.; Varekamp, C. Observation of tropical rain forest trees by airborne high-resolution interferometric radar. *IEEE Trans. Geosci. Remote. Sens.* **2001**, *39*, 584–594. [CrossRef]

18. Deutscher, J.; Perko, R.; Gutjahr, K.-H.; Hirschmugl, M.; Schardt, M. Mapping Tropical Rainforest Canopy Disturbances in 3D by COSMO-SkyMed Spotlight InSAR-Stereo Data to Detect Areas of Forest Degradation. *Remote. Sens.* **2013**, *5*, 648–663. [CrossRef]

19. De Grandi, E.C.; Mitchard, E.; Hoekman, D. Wavelet Based Analysis of TanDEM-X and LiDAR DEMs across a Tropical Vegetation Heterogeneity Gradient Driven by Fire Disturbance in Indonesia. *Remote. Sens.* **2016**, *8*, 641. [CrossRef]

20. Hoekman, D.H.; Kahwage, C. Monitoramento por radar do desmatamento na area central da TIARG. In *Gestão Ambiental e Territorial da Terra Indígena Alto Rio Guamá*; IDEFLOR-Bio: Belém, Brazil, 2017; pp. 327–346, ISBN 978-85-92612-04-7.

21. Hoekman, D. Satellite radar observation of tropical peat swamp forest as a tool for hydrological modelling and environmental protection. *Aquat. Conserv. Mar. Freshw. Ecosyst.* **2007**, *17*, 265–275. [CrossRef]

22. Harris, N.L.; Brown, S.; Hagen, S.C.; Saatchi, S.S.; Petrova, S.; Salas, W.; Hansen, M.C.; Potapov, P.V.; Lotsch, A. Baseline Map of Carbon Emissions from Deforestation in Tropical Regions. *Science* **2012**, *336*, 1573–1576. [CrossRef]

23. Zarin, D.J.; Behie, S.W.; Zelisko, P.M.; Bidochka, M.J. Carbon from Tropical Deforestation. *Science* **2012**, *336*, 1518–1519. [CrossRef]

24. Van Der Werf, G.R.; Morton, D.C.; DeFries, R.S.; Olivier, J.G.J.; Kasibhatla, P.S.; Jackson, R.B.; Collatz, G.J.; Randerson, J.T. CO2 emissions from forest loss. *Nat. Geosci.* **2009**, *2*, 737–738. [CrossRef]

25. Page, S.E.; Siegert, F.; Rieley, J.O.; Boehm, H.-D.V.; Jaya, A.; Limin, S. The amount of carbon released from peat and forest fires in Indonesia during 1997. *Nat. Cell Biol.* **2002**, *420*, 61–65. [CrossRef]

26. Kool, D.M.; Buurman, P.; Hoekman, D.H. Oxidation and compaction of a collapsed peat dome in Central Kalimantan. *Geoderma* **2006**, *137*, 217–225. [CrossRef]

27. ITTO & IUCN. *ITTO/IUCN Guidelines for the Conservation and Sustainable Use of Biodiversity in Tropical Timber Production Forests*; ITTO Policy Development Series No. 17; ITTO: Yokohama, Japan, 2009; ISBN 4-902045-41-9.

28. Vasconcelos, A.; Bernasconi, P.; Guidotti, V.; Silgueiro, V.; Valdiones, A.; Carvalho, T.; Bellfield, H.; Guedes Pinto, L.F. Illegal Deforestation and Brazilian Soy Exports: The Case of Mato Grosso. Available online: http://resources.trase.earth/documents/issuebriefs/TraseIssueBrief4_EN.pdf (accessed on 6 October 2020).

29. van Stokkom, A.; Dallinga, J.; Debuyser, M.; Hoekman, D.; Kooij, B.; Pacheco, P.; Thau, D.; Valkman, S.; Beukeboom, H. An Innovative Early Warning System To Tackle Illegal Deforestation (10667). In Proceedings of the FIG Working Week 2020, Smart surveyors for land and water management, Amsterdam, The Netherlands, 10–14 May 2020.

30. UNFCCC. Reducing Emissions from Deforestation in Developing Countries: Approaches to Stimulate Action. UNFCCC/COP-13 Draft Decision. 2007. Available online: http://unfccc.int/files/meetings/cop_13/application/pdf/cp_redd.pdf (accessed on 2 October 2020).

31. Diniz, C.G.; Souza, A.A.D.A.; Santos, D.C.; Dias, M.C.; Da Luz, N.C.; De Moraes, D.R.V.; Maia, J.S.A.; Gomes, A.R.; Narvaes, I.D.S.; Valeriano, D.M.; et al. DETER-B: The New Amazon Near Real-Time Deforestation Detection System. *IEEE J. Sel. Top. Appl. Earth Obs. Remote. Sens.* **2015**, *8*, 3619–3628. [CrossRef]

32. Sano, E.E.; Freitas, D.M.; Souza, R.A.; Matos, F.L.; Ferreira, G.P. Detecting new deforested areas in the Brazilian Amazon using ALOS-2 PALSAR-2 imageries. In *ALOS Kyoto & Carbon Initiative Science Team Reports Phase 4 (2015–2019)*; JAXA EORC NDX-2019009; Japan Aerospace Exploration Agency, Earth Observation Research Center: Ibaraki, Japan, March 2020; pp. 269–277.

33. Watanabe, M.; Koyama, C.N.; Hayashi, M.; Nagatani, I.; Shimada, M. Early-Stage Deforestation Detection in the Tropics With L-band SAR. *IEEE J. Sel. Top. Appl. Earth Obs. Remote. Sens.* **2018**, *11*, 2127–2133. [CrossRef]

34. Watanabe, M.; Koyama, C.; Hayashi, M.; Nagatani, I.; Tadono, T.; Shimada, M. Improvement of Deforestation Detection Algorithms Used In JJ-FAST. In Proceedings of the IGARSS 2019—2019 IEEE International Geoscience and Remote Sensing Symposium, Yokohama, Japan, 28 July–2 August 2019; pp. 5328–5331.

35. Watanabe, M.; Koyama, C.; Hayashi, M.; Nagatani, I.; Tadono, T.; Shimada, M. JJ-FAST Update. JAXA Kyoto and Carbon Initiative Meeting 26. 2020. Available online: https://www.eorc.jaxa.jp/ALOS/kyoto/jan2020_kc26/pdf/1-07_PKC1_Watanabe.pdf (accessed on 2 October 2020).

36. Rosenqvist, A.; Shimada, M.; Ito, N.; Watanabe, M. ALOS PALSAR: A Pathfinder Mission for Global-Scale Monitoring of the Environment. *IEEE Trans. Geosci. Remote. Sens.* **2007**, *45*, 3307–3316. [CrossRef]

37. Shimada, M.; Itoh, T.; Motooka, T.; Watanabe, M.; Shiraishi, T.; Thapa, R.; Lucas, R. New global forest/non-forest maps from ALOS PALSAR data (2007–2010). *Remote. Sens. Environ.* **2014**, *155*, 13–31. [CrossRef]

38. Koyama, C.N.; Watanabe, M.; Hayashi, M.; Ogawa, T.; Shimada, M. Mapping the spatial-temporal variability of tropical forests by ALOS-2 L-band SAR big data analysis. *Remote. Sens. Environ.* **2019**, *233*, 111372. [CrossRef]

39. Woodhouse, I.H.; Van Der Sanden, J.J.; Hoekman, D.H. Scatterometer observations of seasonal backscatter variation over tropical rain forest. *IEEE Trans. Geosci. Remote. Sens.* **1999**, *37*, 859–861. [CrossRef]

40. Reiche, J.; Hamunyela, E.; Verbesselt, J.; Hoekman, D.; Herold, M. Improving near-real time deforestation monitoring in tropical dry forests by combining dense Sentinel-1 time series with Landsat and ALOS-2 PALSAR-2. *Remote. Sens. Environ.* **2018**, *204*, 147–161. [CrossRef]

41. Lucas, R.; Rosenqvist, A.; Kellndorfer, J.; Hoekman, D.; Shimada, M.; Clewley, D.; Walker, W.; Navarro de Mesquita Junior, H. *Chapter 4: Global forest monitoring with Synthetic Aperture Radar (SAR) data, In Global Forest Monitoring from Earth Observation*; CRC Press, Taylor & Francis Group: Boca Raton, FL, USA, 2013; ISBN 9781466552012.

42. Armston, J.; Brown, S.; Calders, K.; Cutler, M.; Disney, M.; Endo, T.; Falkowski, M.; Goetz, S.; Herold, M.; Hirata, Y.; et al. Status of Evolving Technologies, GOFC-GOLD Sourcebook Section 2.10, Release: December 2016. GOFC-GOLD Land Cover Project Office, Wageningen University, The Netherlands. Available online: http://www.gofcgold.wur.nl/redd/sourcebook/GOFC-GOLD_Sourcebook.pdf (accessed on 6 October 2020).

43. Bouvet, A.; Mermoz, S.; Ballère, M.; Koleck, T.; Le Toan, T. Use of the SAR Shadowing Effect for Deforestation Detection with Sentinel-1 Time Series. *Remote. Sens.* **2018**, *10*, 1250. [CrossRef]

44. Hansen, J.N.; Mitchard, E.T.A.; King, S. Assessing Forest/Non-Forest Separability Using Sentinel-1 C-Band Synthetic Aperture Radar. *Remote. Sens.* **2020**, *12*, 1899. [CrossRef]

45. Cremer, F.K.A.; Urbazaev, M.; Cortes, J.; Truckenbrodt, J.; Schmullius, C.; Thiel, C.J. Potential of Recurrence Metrics from Sentinel-1 Time Series for Deforestation Mapping. *IEEE J. Sel. Top. Appl. Earth Obs. Remote. Sens.* **2020**, 1. [CrossRef]

46. Sica, F.; Pulella, A.; Rizzoli, P. Forest Classification and Deforestation Mapping by Means of Sentinel-1 InSAR Stacks. In Proceedings of the IGARSS 2019—2019 IEEE International Geoscience and Remote Sensing Symposium, Yokohama, Japan, 28 July–2 August 2019; pp. 2635–2638.

47. Quiñones, M.J.; Vissers, M.; Palacios, S.; Hettler, B.; Mancera, J.R. *Mapa de tipos estructurales de Amazonia occidental, frecuencias de inundación y cambios de cobertura de vegetación: 10 años de línea base para el estudio del bioma Amazónico*; Report Amazon Conservation Team and SarVision: Brasília, Brasil, 2019.

48. Quiñones, M.; Vissers, M.; Pacheco-Pascaza, A.M.; Flórez, C.; Estupiñán-Suárez, L.M.; Aponte, C.; Jaramillo, Ú.; Huertas, C.; Hoekman, D. Un enfoque ecosistémico para el análisis de una serie densa de tiempo de imágenes de radar Alos PALSAR, para el mapeo de zonas inundadas en el territorio continental colombiano. *Biota Colomb.* **2016**, *16*, 63–84. [CrossRef]

49. Flórez, C.; Estupiñán-Suárez, L.M.; Rojas, S.; Aponte, C.; Quiñones, M.; Acevedo, Ó.; Vilardy, S.; Jaramillo, Ú. Identificación espacial de los sistemas de humedales continentales de Colombia. *Biota Colomb.* **2016**, *16*, 44–62. [CrossRef]

50. Di Gregorio, A.; Jansen, L.J.M. *Land Cover Classification System (LCCS): Classification Concepts and User Manual Environment and Natural Resources Service, GCP/RAF/287/ITA Africover—East Africa Project and Soil Resources, Management and Conservation Service*; FAO: Rome, Italy, 2000.

51. Quinones, M.; Sartika, L.; Kooij, B. Brief Technical Report WWF-EWS Project Phase 2. Baseline Map 2015–2019 & Oil Palm Map 2018, Borneo. SarVision Report, WWF Contract, SarVision, Wageningen, The Netherlands. 2020. Available online: https://www.sarvision.nl/contact/ (accessed on 6 October 2020).

52. Roy, D.P.; Li, J.; Zhang, H.K.; Yan, L.; Huang, H.; Li, Z. Examination of Sentinel-2A multi-spectral instrument (MSI) reflectance anisotropy and the suitability of a general method to normalize MSI reflectance to nadir BRDF adjusted reflectance. *Remote. Sens. Environ.* **2017**, *199*, 25–38. [CrossRef]

53. Hoekman, D.; Reiche, J. Multi-model radiometric slope correction of SAR images of complex terrain using a two-stage semi-empirical approach. *Remote. Sens. Environ.* **2015**, *156*, 1–10. [CrossRef]

54. Torres, R.; Snoeij, P.; Geudtner, D.; Bibby, D.; Davidson, M.; Attema, E.; Potin, P.; Rommen, B.; Floury, N.; Brown, M.; et al. GMES Sentinel-1 mission. *Remote. Sens. Environ.* **2012**, *120*, 9–24. [CrossRef]

55. Quegan, S.; Yu, J.J. Filtering of multichannel SAR images. *IEEE Trans. Geosci. Remote. Sens.* **2001**, *39*, 2373–2379. [CrossRef]

56. Lopes, A.; Touzi, R.; Nezry, E. Adaptive speckle filters and scene heterogeneity. *IEEE Trans. Geosci. Remote. Sens.* **1990**, *28*, 992–1000. [CrossRef]

57. Hoekman, D.H. Speckle ensemble statistics of logarithmically scaled data (radar). *IEEE Trans. Geosci. Remote. Sens.* **1991**, *29*, 180–182. [CrossRef]

58. Reiche, J.; De Bruin, S.; Hoekman, D.; Verbesselt, J.; Herold, M. A Bayesian Approach to Combine Landsat and ALOS PALSAR Time Series for Near Real-Time Deforestation Detection. *Remote. Sens.* **2015**, *7*, 4973–4996. [CrossRef]

59. Schlund, M.; Von Poncet, F.; Kuntz, S.; Schmullius, C.; Hoekman, D.H. TanDEM-X data for aboveground biomass retrieval in a tropical peat swamp forest. *Remote. Sens. Environ.* **2015**, *158*, 255–266. [CrossRef]

60. Ferraz, A.; Saatchi, S.S.; Xu, L.; Hagen, S.C.; Chave, J.; Yu, Y.; Meyer, V.; Garcia, M.; Silva, C.A.; Roswintiart, O.; et al. Carbon storage potential in degraded forests of Kalimantan, Indonesia. *Environ. Res. Lett.* **2018**, *13*, 095001. [CrossRef]

61. Varekamp, C.; Hoekman, D.H. High-resolution InSAR image simulation for forest canopies. *IEEE Trans. Geosci. Remote. Sens.* **2002**, *40*, 1648–1655. [CrossRef]

62. Haralick, R. Ridges and Valleys on Digital Images. *Comput. Vis. Graph. Image Process.* **1983**, *22*, 28–38. [CrossRef]

63. López, A.M.; Lumbreras, F.; Serrat, J.; Villanueva, J. Evaluation of methods for ridge and valley detection. *IEEE Trans. Pattern Anal. Mach. Intell.* **1999**, *21*, 327–335. [CrossRef]